One step superparamagnetic iron oxide nanoparticles by a microwave process: optimization of microwave parameters with an experimental design

Thomas Girardet, Morgane Kessler, Sylvie Migot, Lionel Aranda, Sebastien Diliberto, Stéphane Suire, Tom Ferté, Sebastien Hupont, Franck Cleymand, Solenne Fleutot

One step superparamagnetic iron oxide nanoparticles by a microwave process: optimization of microwave parameters with an experimental design.

*Thomas Girardet, Morgane Kessler, Sylvie Migot, Lionel Aranda, Sébastien Diliberto, Stéphane Suire, Tom Ferté, Sébastien Hupont, Franck Cleymand, Solenne Fleutot**

Thomas Girardet, Morgane Kessler, Sylvie Migot, Lionel Aranda, Sébastien Diliberto, Stéphane Suire, Tom Ferté, Sébastien Hupont, Franck Cleymand, Solenne Fleutot
Institut Jean Lamour, CNRS University of Lorraine, 4 allée André Guinier, 54 000 Nancy, France
E-mail: solenne.fleutot@univ-lorraine.fr

Keywords: iron oxide nanoparticle, experimental design, superparamagnetism, microwave process

Superparamagnetic iron oxide nanoparticles (SPIONs) are nanoparticles used in a lot of applications such as batteries, biomedical, … To obtain these nanoparticles, several techniques exist such as coprecipitation, thermal decomposition, sol-gel process but they have some advantages (synthesis in a water media, high crystallinity, high monodispersity) and disadvantages (using organic solvent, large distribution of size, poor crystallinity). The goal of this work is to synthesize SPIONs for biomedical applications (for example as contrast agent for the MRI): SPIONs should be stable in an aqueous media, monodisperse and have good crystallinity and magnetic properties. To achieve this result, microwave process is carried out. However, any study describes the microwave parameter on the synthesis of the nanoparticles. This work offers to determine the best conditions of the microwave to obtain ideal SPIONs for MRI. For this, an experimental design is carried out to determine these parameters thanks to different techniques of characterization (Transmission Electronic Microscopy, Dynamic Light Scattering, X-Ray Diffraction, Thermogravimetric Analysis, magnetic characterizations). With the different results of these characterizations, the best conditions of the microwave are determined, and a simulation of all experiments is realised with a surface response.

1. Introduction

The use of nanoparticles is becoming more and more common in various applications such as data storage,[1] batteries,[2] biomedical. Indeed, thanks to the high ratio between surface and volume, the nanoparticles are good candidates for these applications. For biomedical

applications, nanoparticles are used for the diagnosis (medical imaging such as Magnetic Resonance Imaging MRI, Positron Emission Tomography PET),[3–5] for therapy (e.g. hyperthermia for the cancer treatment)[6,7] or both with the vectorization of an active substance with nanoparticles directly to damaged cells.[8,9] For this purpose, different nanoparticles can be used according to their properties, their biocompatibility and their no-toxicity. The most commonly used nanoparticles are silver, gold, gadolinium, iron.[10–13]

Thanks to the magnetic properties of certain elements, the possibility of used these nanoparticles in different fields is increasing. For example, magnetic nanoparticles are used as contrast agent (CA) for the MRI imaging to increase the contrast and to reduce the time of analysis. Gadolinium (Gd^{3+}) and iron oxide (Fe_3O_4) are the most important nanoparticles for this application.[12,14,15] Indeed, due to the strong magnetization, Gd^{3+} is one of the best contrast agents for MRI: the longitudinal relaxation time (called T_1) is shortened and so the signal strength is increasing. The main disadvantages is the toxicity of this paramagnetic centre in particular with the brain.[16,17] To avoid this toxicity, an organic layer is grafted around the gadolinium core.[18] Another strategy consists to use iron oxide as CA for MRI imaging because iron oxide are less toxic: this inorganic compound has a good magnetization.[19,20] They are different types of iron oxide but magnetite (Fe_3O_4) and maghemite (γ-Fe_2O_3) are often used due to their high magnetization. In addition, in function the size of the iron oxide nanoparticle, different magnetic behaviours are present. If the size is greater than 20 nm, iron oxide nanoparticles are in a ferrimagnetic state. [21] If the size is below than 20 nm, a superparamagnetic behaviour is present: the magnetization is zero when the applied magnetic field is equal to 0 Tesla. These nanoparticles with this magnetic state are used in MRI as CA: the transverse relaxation time (called T_2) is shorten and the signal strength is reduced.[22] It is for this reason that we had chosen the synthesis of iron oxide nanoparticles for this work.

Superparamagnetic Iron Oxide Nanoparticles (SPIONs) can be synthesized by different methods such as coprecipitation,[23–25] thermal decomposition,[26,27], hydrothermal, [28,29] sol-gel process[30] but each synthesis has its advantages and disadvantages and can modify the physico-chemical properties and therefore the desired applications. For example, SPIONs can be obtain by thermal decomposition: SPIONs have a narrow size distribution, a good crystallinity and the control of the size and the shape is easy.[31,32] However, SPIONs are stable in an organic media due to the ligands present around the inorganic core (generally fatty acid such as oleic acid, ….) and several steps are mandatory to eliminate the presence of these organic solvent (transfer phase in an aqueous media, create a micellar system, …).[33,34]
For that, the coprecipitation synthesis is chosen because it allows to obtain SPIONs stable in water media for an using as CA. Indeed, this synthesis is one of the more used synthesis to obtain iron oxide nanoparticles because it is easy and quickly.[23–25] A mixture of iron salts (usually a mixture of iron chloride II and iron chloride III) with a base is realised. But, with these conditions, SPIONs obtained by this technique are aggregate and without a control of the shape and the size. To overcome these problems, an addition of a ligand (polyvinyl alcohol PVA, polyethylene glycol PEG, citric acid, …) is necessary.[35–37] To reduce this size distribution even further, a new synthesis directly in water is developed since a few years: the microwave synthesis.[38,39] Thanks to the microwave irradiations, a control of the temperature within the reactor is carried out: this temperature control allows to obtain monodisperse SPIONs.[40] More and more publications about the synthesis of inorganic nanoparticles are published since 2000' but just a few publications talk about the microwave parameters and their influence on the synthesis and the physico-chemical properties of SPIONs.[41] Indeed, these parameters as time of the synthesis, the temperature, the power of the microwave and the stirring

can modify several parameters of SPIONs (mean diameter, lattice parameter, saturation magnetization).

In this study, we want to investigate and predict the best parameters of the microwave on a synthesis of SPIONs using a microwave process with an addition of citrate as ligand. For this, a statistical approach is carried out with an experimental design (ED).[42–45] The chemical conditions of the synthesis were reported previously and remained fixed for this study: only the microwave parameters were modified in this study.[46] All synthesis were operated in the same conditions. To predict the best conditions of microwave parameters, different technique of characterizations is carried out. Then, with the answer of these techniques, a prediction of these answers was analysed to determine how SPIONs must be synthesized for MRI applications.

2. Results and Discussion

SPIONs has been synthesized according to the parameters described on **Table S1**. For the rest of this work, an example of a sample ($S6_{3A}$) and its characterizations are presented and the other sample with their characterizations are summarized on **Table S2**.
A TEM micrograph of $S6_{3A}$ is presented on **Figure 1**.a with its histogram of size distribution (**Figure 1**.b). SPIONs obtained by microwave synthesis are monodispersed, with no or a little aggregation thanks to the organic layer around the inorganic core (another micrograph is present on **Figure S2**). The mean diameter of $S6_{3A}$ obtained by the size distribution is equal to 2.77 ± 0.91 nm. From all samples, the size is between 2.68 nm and 3.57 nm (**Figure 1**.c). This diameter is an important response of the ED. Given the diameter of each SPION, this parameter should be maximised in order to achieve a higher chance of good crystallinity and of high magnetization saturation. In addition, with the TEM characterization, another response can be obtained: the standard deviation. One objective of this work is to obtain isolated iron oxide nanoparticles stable in aqueous solution and with the same size: the standard deviation σ_{TEM} should be minimized. For all samples, σ_{TEM} is between 0.83 nm to 1.32 nm (**Figure 1**.d).

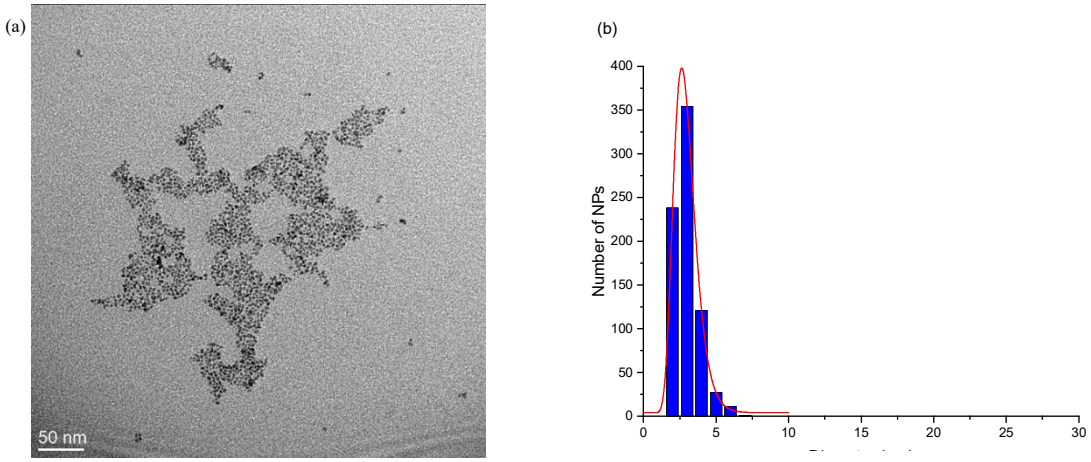

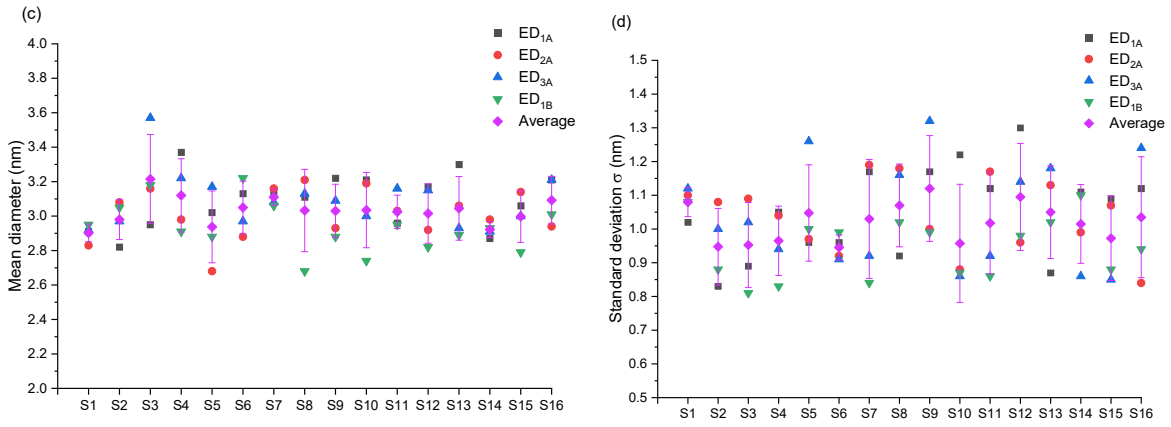

Figure 1: TEM image of $S6_{3A}$ (a) and its size distribution (b). To obtain the mean diameter, a lognormal fit (red line) was carried out and the size was 2.77 ± 0.91 nm. A distribution of each mean diameter d_{TEM} (c) and of standard deviation σ_{TEM} (d) of all samples of ED are represented with the average (pink) and the corresponding standard deviation.

Then, to determine the stability of iron oxide nanoparticles in an aqueous solution and the hydrodynamic diameter (i.e. the diameter of the inorganic core plus the organic layer and the solvation sphere), DLS measurements were carried out. A comparison between the diameter of the inorganic core and the hydrodynamic diameter of $S6_{3A}$ is described on **Figure 2**.a. The hydrodynamic diameter of these SPIONs is equal to 8.5 ± 2.3 nm. Compared to the mean diameter of the inorganic core, the hydrodynamic diameter is higher. This increase of the size is due to the presence of ligands around the inorganic core or an aggregation of SPIONs. However, with the TEM micrograph (**Figure 1**.a), no aggregation is visible: the increasing of diameter is due to the organic layer. For other samples of the ED, the hydrodynamic diameter is between 5.6 nm and 26.5 nm and are shown on **Figure 2**.b. For the biomedical applications and especially for CA, the hydrodynamic diameter d_{DLS} should be as large as possible but without aggregation to avoid blocking the blood vessels: this parameter should be maximised in the ED. Indeed, the efficacity of SPIONs as CA is dependent on the hydrodynamic diameter: as the hydrodynamic diameter increases, the efficiency increases too.[47,48]

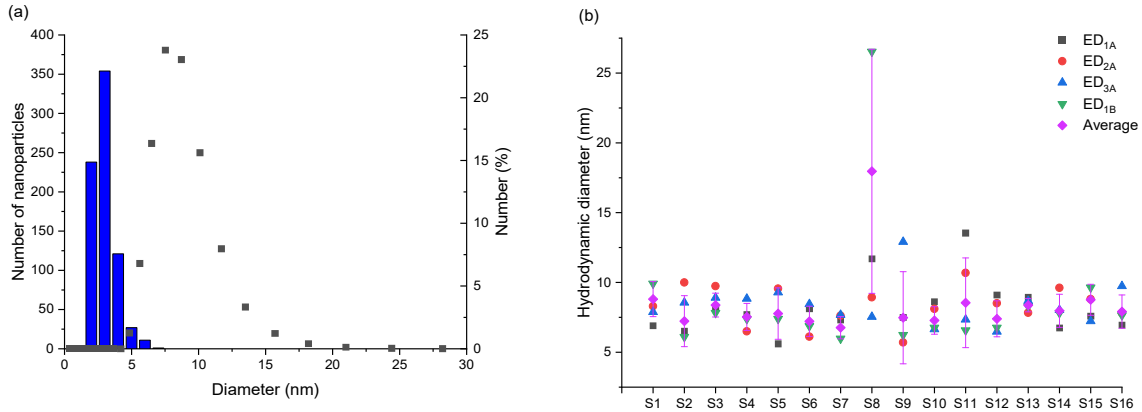

Figure 2: size distribution with the hydrodynamic diameter (8.5 ± 2.3 nm) in function of the number of $S6_{3A}$ (a) and the distribution of each hydrodynamic diameter d_{DLS} of all samples of ED with the average (pink) and their corresponding standard deviation (b).

To verify the crystallographic structure of the inorganic core, XRD patterns measurements were carried out. The principal iron oxide, magnetite Fe_3O_4 and maghemite γ-Fe_2O_3, crystallize in

the same cubic crystal structure ($F_{d\bar{3}m}$): this structure is an inverse spinel. The XRD pattern of $S6_{3A}$ is shown on **Figure 3**.a. The main peaks of iron oxide are indexed according to the spinel structure. To determine if SPIONs are magnetite, maghemite or sub-stoichiometric magnetite ($Fe_{3-\delta}O_4$ with δ the stoichiometric deviation), the lattice parameter a_{XRD} was calculated with the main peaks. For almost the samples, the lattice parameter a_{XRD} is between 8.395 Å (lattice parameter of pure Fe_3O_4) and 8.354 Å (lattice parameter of pure γ-Fe_2O_3) (**figure S3**). For $S6_{3A}$, the lattice parameter is equal to 8.357 ± 0.005 Å. For the other samples, a_{XRD} is between 8.353 Å and 8.432 Å (**Figure 3**.b). For the ED, a_{XRD} should be near to the lattice parameter of magnetite (i.e. 8.395 Å) because magnetite has a higher magnetization than to maghemite.
In addition, with XRD measurements, the crystallite size can be calculated. Indeed, each nanoparticle can be assimilated to one crystal because a nanoparticle is composed of a single domain. Thanks to the Debye-Scherrer equation and the position of the mean peak of the patterns (the 311 plane), the crystal size t_{XRD} can be calculated. For $S6_{3A}$, t_{XRD} is equal to 3.51 nm. For the other samples, t_{XRD} is between 3.02 nm and 4.01 nm (**Figure 3**.c). For the ED, this parameter should be maximised to increase the magnetization saturation.

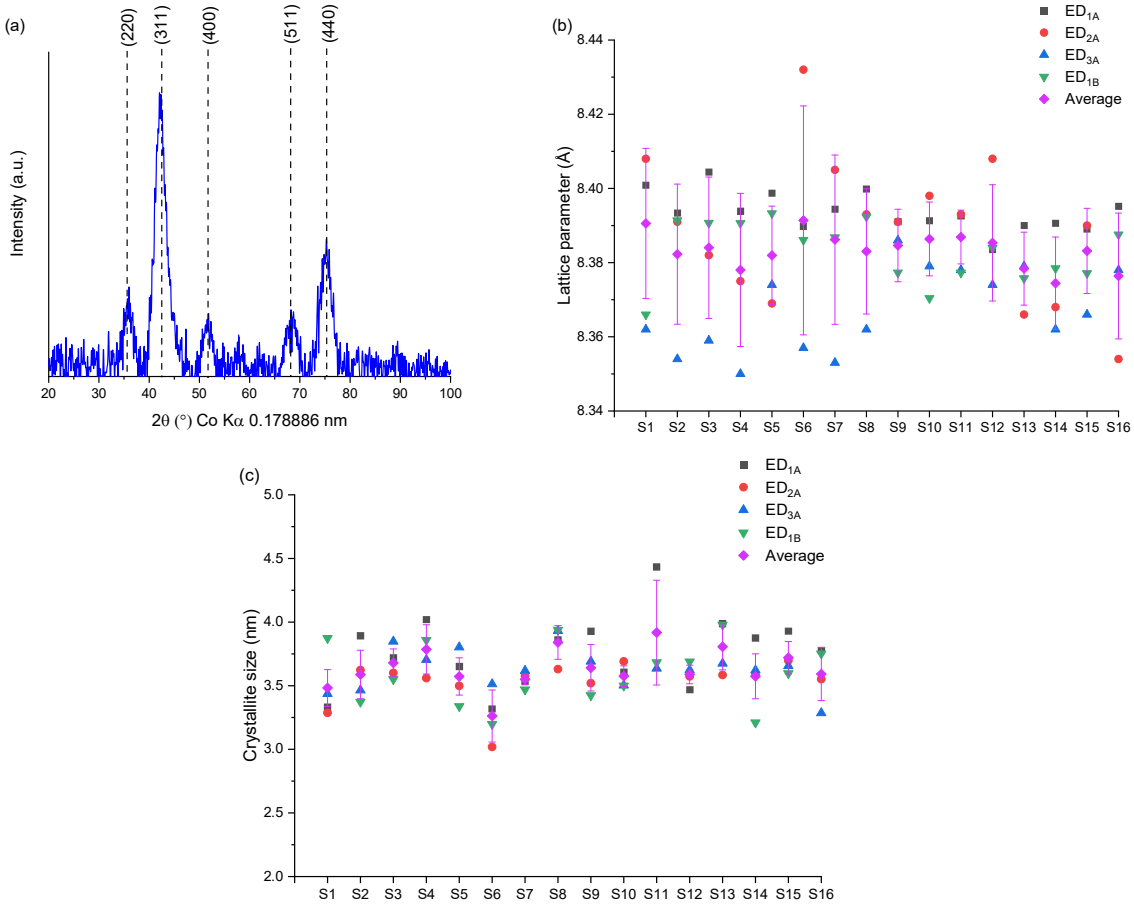

Figure 3: XRD spectra of $S6_{3A}$ (a) and the distribution of lattice parameter a_{XRD} (b) and of crystallite size t_{XRD} (c) of each sample of the ED with the average (pink) and their corresponding standard deviation.

To justify the presence of an assumed organic layer with DLS measurements, a thermogravimetric analysis (TGA) measurements were carried out. An example of TGA (of $S6_{3A}$) curve is present on **Figure 4**.a and other TGA curves are one **Figure S4**: all TGA curves are the same behaviour in function of the temperature. During the heating of the sample, three steps were present. The first began at room temperature and finished around 150°C and corresponded to the evaporation of water. The second step, and the more important, is between

180°C and 250°C and corresponded to the decomposition of the citrate. Indeed, with a comparison with a TGA curve of citric acid (**Figure S4**), the weight loss is similar. Finally, the last stage around 300°C is considered to be decomposition of the last remaining chains. The percentage of ligand $\%_{lig}$ of $S6_{3A}$ is equal to 35%. The percentage of the other samples of ED are between 16% and 39% of ligands (**Figure 4**.b). This parameter should be around 30%/35% to obtain a good stability of SPIONs in an aqueous solution.

Another technique of characterization to confirm the presence of citrate around the iron oxide core is the FTIR, shown on **Figure S5** for the sample $S6_{3A}$. For all samples of ED, the same vibrational bands are observed. At high wavenumber, a large band from 3500 to 3000 cm^{-1} corresponds to the stretching vibration of O-H of the hydroxyl group in citrate and absorbed water. At 1610 cm^{-1} and at 1415 cm^{-1}, two intensive bands are present and corresponded respectively to the asymmetric and symmetric stretching of carboxylate groups. In addition, these two bands were offset by 30 cm^{-1} due to the chemisorption of citrate on the surface of SPIONs.[49] The presence of these carboxylate groups is confirmed by the stretching of C-O at 1260 cm^{-1}. At the low wavenumber, the type of iron oxide nanoparticles can be determined. Indeed, if there is only one intense peak around 580 cm^{-1}, the major phase is magnetite and if there are few peaks from 400 to 800 cm^{-1}, the major phase is maghemite.[50,51] For all samples of the ED, there are an intense peak at 580 cm^{-1} thus confirming the presence of magnetite, but other peaks are present: in this case, the major phase of the inorganic core is magnetite with a slight oxidation which corresponds to sub stoichiometric magnetite $Fe_{3-\delta}O_4$.

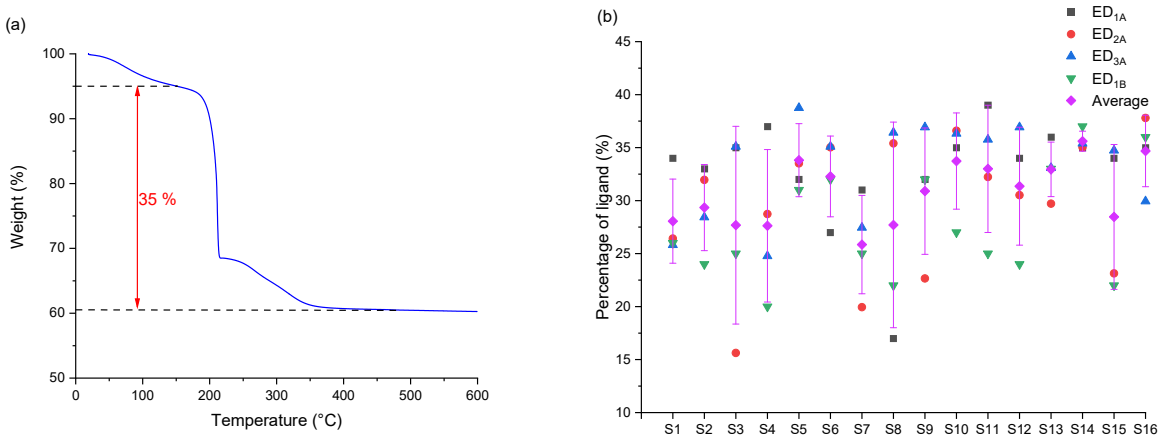

Figure 4: thermogravimetric analysis from 20°C to 600°C of $S6_{3A}$ (a) and the distribution of percentage of ligands $\%_{lig}$ of each sample of the ED with the average (pink) and their corresponding standard deviation (b).

The last essential characterization of our SPIONs is the magnetic characterizations. Indeed, the magnetic state is an important parameter for the use of these nanoparticles as CA. The first measurement is a magnetization cycle at room temperature: a magnetic field is applied from 50 000 Oe (1 Tesla = 10 000 Oe) to -50 000 Oe and from -50 000 Oe to 50 000 Oe. If the magnetic state is a cooperative magnetism, when the magnetic field changes, a coercive field will then appear: a hysteresis loop is generated. If the magnetic state is a no cooperative magnetism such as superparamagnetism, any hysteresis is generated: when the applied magnetic field is zero, the magnetic moment is also zero. In our case and for all samples of the ED, any hysteresis is present on the magnetic cycle at room temperature: all samples are in a supereparamagnetic state at 300K (**Figure 5**.a and **Figure S6**). The second information given by these curves is the magnetization saturation M_S (i.e the maximum of the magnetic moment). The M_S of a bulk of maghemite γ-Fe_2O_3 is 74 $emu.g^{-1}$ and for a bulk of magnetite Fe_3O_4 is 92 $emu.g^{-1}$. The goal is to maximise the value of M_S to improve the efficacity of SPIONs as CA.

The magnetic cycle of $S6_{3A}$ is shown of **Figure 5**.a. The M_S of samples of the ED are between 18 emu.g^{-1} and 65 emu.g^{-1} (**Figure 5**.b). To confirm the superparamagnetic state, magnetic cycles are carried out at 5K (**Figure 5**.c). Indeed, at this temperature, the magnetic moment is blocked: the magnetic behaviour is similar to a cooperative magnetism; a hysteresis is therefore present when the applied magnetic field is changed. The insert on **Figure 5**.c showed this hysteresis for $S6_{3A}$ and is present for all samples of the ED. As the magnetic moment is blocked, the M_S value is therefore higher as shown the distribution of M_S at 5K (**Figure 5**.d): the M_S values are between 43 emu.g^{-1} to 95 emu.g^{-1}. As for the M_S value at 300K, the M_S at 5K should be maximise for a use as CA.

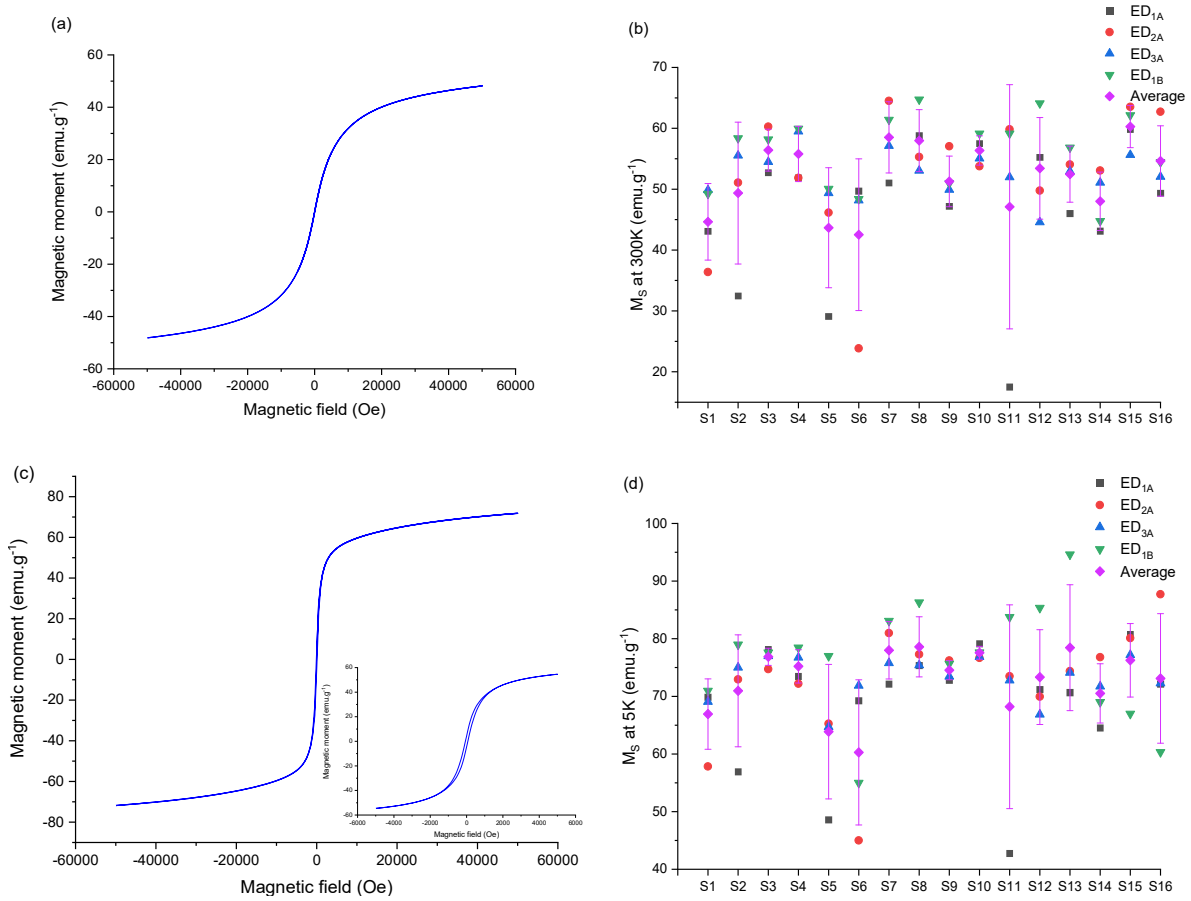

Figure 5: magnetic cycle of $S6_{3A}$ at 300K (a), the distribution of M_S values at 300K of each sample of the ED with the average (pink) with their corresponding standard deviation (b), magnetic cycle of $S6_{3A}$ at 5K and in insert a zoom to see the hysteresis (c) and the distribution of M_S at 5K of each sample of the ED with the average (pink) with their corresponding standard deviation (d).

At 300K, all nanoparticles studied in this work are in a superparamagnetic state and are in a blocked magnetic state at 5K. However, the transition temperature between these two states is not known. To determine this temperature, called blocking temperature T_B, ZFC-FC curves are carried out. Generally, T_B is assimilated to the maximum of the ZFC curve (i.e. the curve from 5K to 300K). However, this value is not the exact value because we assume that all SPIONs have the same size. There is a distribution of size of SPIONs, so there is a blocking temperature distribution too: a blocking region should be considered. The exactly T_B is thus determined by means of Monte-Carlo simulations.[52] For ease of reference, we therefore consider T_B to be the maximum of the ZFC curve. The ZFC-FC curve of $S6_{3A}$ is shown on **Figure 6**.a and other examples are present on **Figure S7**. The value of T_B is equal to 13K. For the other samples, T_B is between 11K and 46K (**Figure 6**.b). In addition, as mentioned above, the ZFC-FC curve

corresponds to a distribution of T_B. This distribution can be to compare with the size distribution obtained with TEM images: if the size distribution is large, the distribution of T_B must be large. For $S6_{3A}$, the size distribution is narrow like the distribution of T_B.

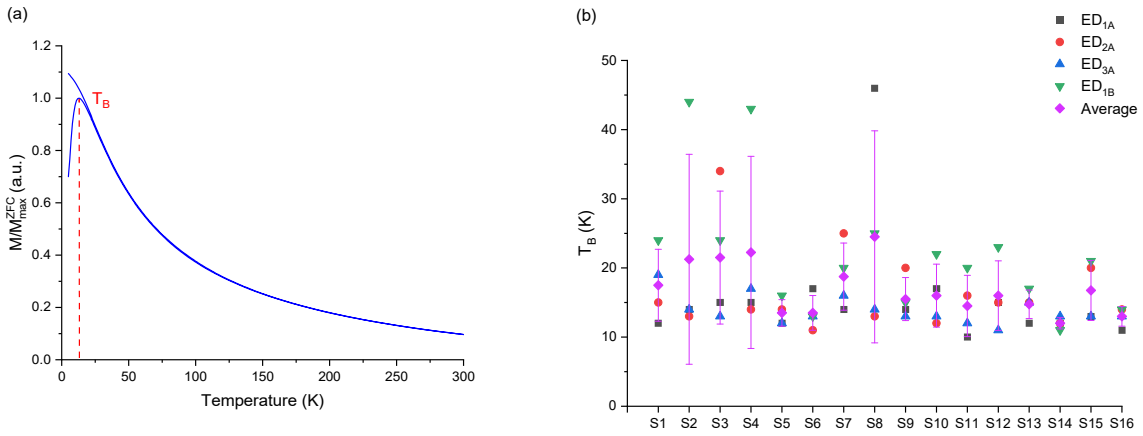

Figure 6: ZFC-FC curve of $S6_{3A}$ with a T_B = 13K (a) and the distribution of T_B of each sample of the ED with the average (pink) and their corresponding standard deviation (b).

Thanks all these characterizations, the different responses (the mean diameter d_{TEM}, the standard deviation in TEM σ_{TEM}, the hydrodynamic diameter d_{DLS}, the lattice parameter a_{XRD}, the crystallite size t_{XRD}, the percentage of ligands $\%_{lig}$, the magnetization saturation at 300K M_S_300K and at 5K M_s_5K and the blocking temperature T_B) for our ED have been obtained and will allow us to determine the best microwave parameters to synthesize iron oxide nanoparticles for a use as CA. However, in view of the number of results for each response, a search of outliers is carried out thanks a Dixon's test (described on Figure S8). This test allows to discriminate the extreme values. With a threshold of 0.01 ($r_{4;0.99}$ = 0.889), a few values are removed: these values are crossed out on **Table S2**.

To prove the repeatability, as mentioned above, the ED was repeated three times by the same operator. After this repeatability, an ANOVA (Analysis of Variances) is carried out to check if the different average of the different repeatability (ED_{1A}, ED_{2A} and ED_{3A}) are similar or not. If the average of each repeatability is similar, the ED is repeatable. The different ANOVA of each response are present on **Table S3**. The difference between each ED is calculated and compared with the limit of repeatability (calculated from the sum of squared differences). If the difference is below to the limit of repeatability, we can hypothesize that the synthesis is repeatable. In this study, for all samples (16 samples per each ED) and for all responses, the difference between each ED is below to the limit of repeatability: the ED is so repeatable.

For the reproducibility, the same operation is realised but with the average of two different operators (i.e. with the average of ED_{yA} y = 1;2;3 and with ED_{1B}). The results of ANOVA are present on **Table S4**. The same calculi are carried out than the repeatability and for each sample and each response, the difference between ED is below to the limit of reproducibility: the ED is maybe reproducible. To totally confirm this hypothesis, another operator in another lab must carry out this ED and the same physico-chemical characterizations.

After to prove the repeatability and the reproducibility of the ED, the determination of the best microwave parameters for an application as CA is realized. For this, the average of each level of each factor is calculated. Thus, thanks to an effects diagram, the variations between the different levels of a factor become visual. For example, for the microwave power (factor D) at

650 W (level 3), the value is equal to the average of the response of S3, S5, 0 and S16. All averages of each response are summarised on **Table S5**. The different effects diagrams are shown on **Figure 7**.

After determining how the responses should be (maximised, minimised, or close to a value), an optimisation of the microwave parameters is obtained according to this response. Thus, the mean diameter d_{TEM} should be maximised (in view of the sizes obtained) (**Figure 7**.a), the standard deviation σ_{TEM} should be minimized (**Figure 7**.b), the hydrodynamic diameter d_{DLS} should be maximised (**Figure 7**.c), the lattice parameter a_{XRD} should be near to 8.395 Å (the lattice parameter of magnetite Fe_3O_4) because magnetite has a higher magnetization and therefore allows to increase the efficiency as CA (**Figure 7**.d). Then, in accordance with the mean diameter d_{TEM}, the crystallite size should be maximised (in view of the sizes obtained) (**Figure 7**.e). For a good stability in an aqueous media, the percentage of ligands $\%_{lig}$ should be near to 30/32% (**Figure 7**.f). Finally, for the magnetic properties, the magnetisation saturation M_s at 300K (**Figure 7**.g) and at 5K (**Figure 7**.h) should be maximised due to the potential application as CA. For the blocking temperature T_B, this parameter should be minimised because generally when T_B is high, aggregates can appear (**Figure 7**.i).

For example, one goal of this study is to obtain monodisperse SPIONs: the size distribution should be narrow. So, to validate this criterion, the standard deviation σ_{TEM} should be minimised. With the effects diagram of σ_{TEM} (**Figure 7**.b), a minimum of the standard deviation is obtained when the ramp time is 5 min (factor A, level 1), the temperature is 90°C (factor B, level 1), the stage time is 40 min (factor C, level 4), the microwave power is 650 W (factor D, level 3) and without a stirring during the synthesis (factor E, level 1). However, in order to obtain reproducible and repeatable synthesis, the variance must also be minimised for all responses. The different variances of each response in function of the factor are shown on **Figure S9**.

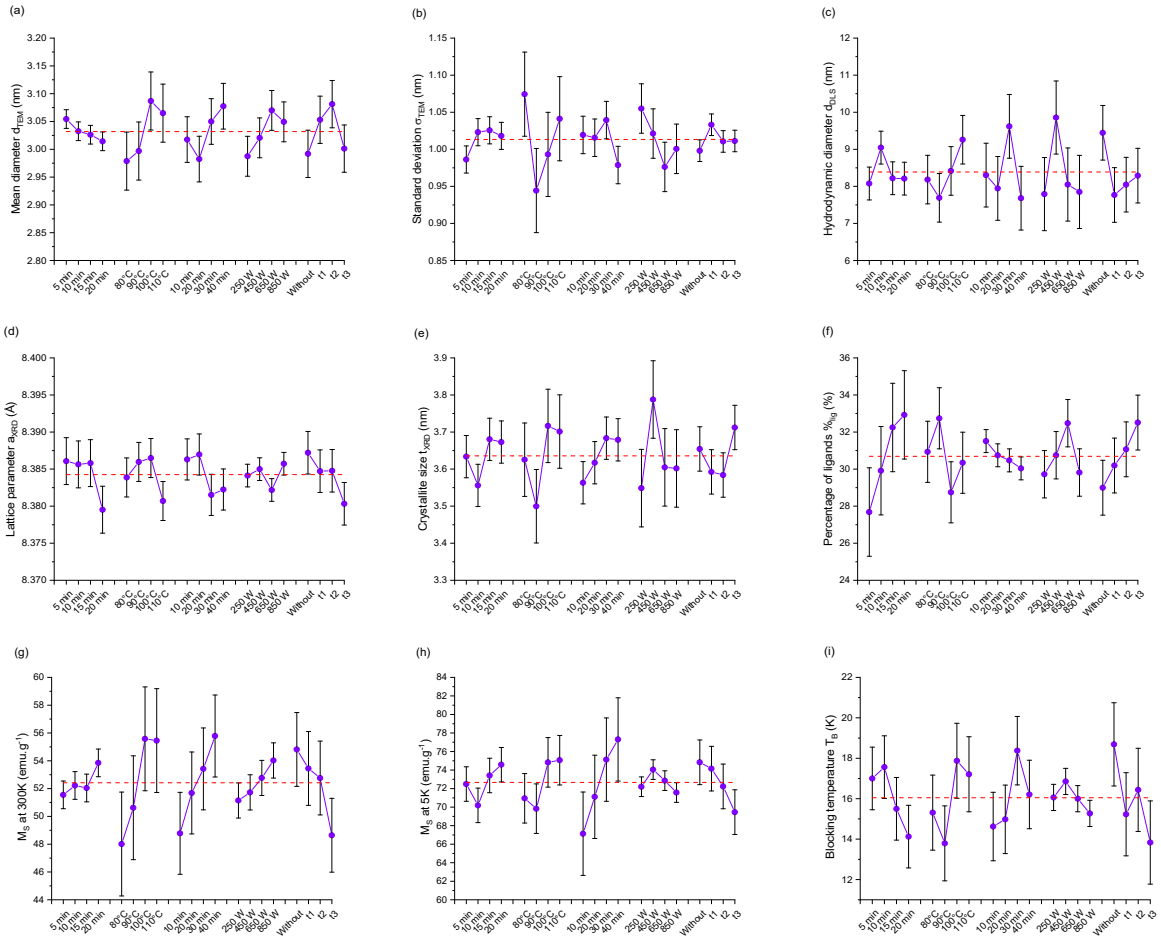

Figure 7: effect diagrams of the different responses of the ED: mean diameter d_{TEM} (a), standard deviation σ_{TEM} (b), hydrodynamic diameter d_{DLS} (c), lattice parameter a_{XRD} (d), crystallite size t_{XRD} (e), percentage of ligands $\%_{lig}$ (f), the magnetization saturation at 300K M_S_300K (g), the magnetization saturation at 5K M_S_5K (h) and the blocking temperature T_B (i) with their average (red dash).

Taking into account the variance and the responses, the optimized microwave parameters for each response can be determined and are summarized on **Table 1**. Several parameters are similar between the different responses as for the factor E: the best condition is to realize the synthesis without a stirring. For the factor D, the level which is optimal for almost responses is at 850 W. For the other factors, a trend can be identified. Indeed, with a ramp time of 20 minutes (factor A, level 4) at 100°C or 110°C (factor B, level 3 or 4) and a stage time of 40 minutes, SPIONs synthesised with these parameters will be optimized for an application as CA.
However, a certain hindsight must be taken into account based on the statistical results. Indeed, in according to the ED, any stirring allows to obtain better SPIONs for the application as CA: the absence of stirring will generate an aggregation of SPIONs. If there is an aggregation of these nanoparticles, the magnetization saturation will be increases because there will be a set of magnetic nanoparticles generating more magnetism.

Table 1: table of the best microwave conditions for each response.

Factor	d_{TEM}	σ_{TEM}	d_{DLS}	a_{XRD}	t_{XRD}	$\%_{lig}$	M_s 300K	M_S 5K	T_B
A	10 min (2)	5 min (1)	10 min (2)	15 min (3)	20 min (4)	10 or 15 min (2 or 3)	20 min (4)	20 min (4)	20 min (4)
B	100°C (3)	90°C (2)	100°C or 110°C (3 or 4)	100°C (3)	110°C (4)	80°C (1)	110°C (4)	110°C (4)	90°C (3)
C	30 or 40 min (3 or 4)	40 min (4)	30 min (3)	20 min (2)	40 min (4)	40 min (4)	40 min (4)	30 or 40 min (3 or 4)	10 or 20 min (1 or 2)
D	850 W (4)	650 or 850 W (3 or 4)	450 W (2)	450 W (2)	650 W (3)	250 W (1)	850 W (4)	250 or 650 W (1 or 3)	850 W (4)
E	t_1 (2)	without (1)	without (1)	without (1)	without (1)	t_1 (2)	without (1)	without (1)	t_3 (4)

Thanks to these averages of each response (which are constructed the different effects diagrams), a simulation of the 1024 experiments (i.e. all experiments with all levels for each factor) is realized using the law of additivity of responses. This law consists of adding the mean of different factors at a specific level with the main average and the whole is divided by the number of factors and the main average. For the experiment with the following conditions (ramp time of 15 minutes, temperature at 80°C, stage time of 20 minutes, microwave power at 850 W and without stirring i.e. A = 3, B = 1, C = 2, D = 4 and E = 1), the calculated response of the mean diameter d_{TEM} is equal to (Equation 1):

$$d_{TEM}(3;1;2;4;1) = \frac{\bar{x}_{A=3} + \bar{x}_{B=1} + \bar{x}_{C=2} + \bar{x}_{D=4} + \bar{x}_{E=1} + \bar{x}_{d_{TEM}}}{6} \quad (1)$$

With $\bar{x}_{A=3}$ the average of d_{TEM} when the factor A is equal to 3 (i.e. when the ramp time is 15 minutes, the average is equal to d_{TEM} of S1, S2, S3 and S4. For $\bar{x}_{B=1}$, the average is equal to the average of d_{TEM} of S1, S5, S9 and S13. For $\bar{x}_{C=2}$, the average is equal to the average of d_{TEM} of S2, S5, S12 and S15. For $\bar{x}_{D=4}$, the average is equal to the average of d_{TEM} of S4, S6, S9 and S15. For $\bar{x}_{D=1}$, the average is equal to the average of d_{TEM} of S1, S8, S10 and S15. Finally, $\bar{x}_{d_{TEM}}$ is the total average of each value of d_{TEM} from the ED.

Thanks this different calculated values, the simulation of each response in function of the level of each factor is carried out and surface responses are obtained (**Figure 8**). In addition, thanks to these simulated data, the variation of one factor (with the other fixed) in function of each response is possible to be check (**Table S6**). For example, when the microwave power increases, the magnetic saturation at 300K increases too. All factors in function of each response are reported on **Table S6**.
With this surface response, the last step for an experimental design can be carried out: the validation of the ED with another experiments. Indeed, three randomised experiments and three choose experiments are realised. The conditions are summarized on **Table S7**. Then, the values of the responses are reported on the surface response and the difference between the theoretical response and the experimental response is observed. All the values of each response of these last experiments are reported on **Table S8**. In general, the responses of the different experiment are near to the theoretical values. However, of the six randomised experiments, two have outliers: these differences are due to the percentage of ligand. Indeed, if the percentage of ligand is high, a matrix of this ligand appeared: the mean size is low, the hydrodynamic diameter increases, the magnetic properties decrease. In addition, an oxidation phenomenon occurs. This phenomenon is visible thanks to the magnetic characterization: the hysteresis is higher than the other synthetised nanoparticles and when a magnetic field is applied (4 Tesla) for a magnetic cycle at 5K, the left coercive field is higher than the left coercive field without a magnetic field. This increasing corresponds to the presence of another magnetic state: for our case, this other magnetic state is due to the presence of maghemite. Finally, when the percentage of ligands is low, the magnetic properties decrease too. For the other samples, the percentage of ligands is between 32% and 35%: the different other responses are near to their theoretical values obtained with the ED.

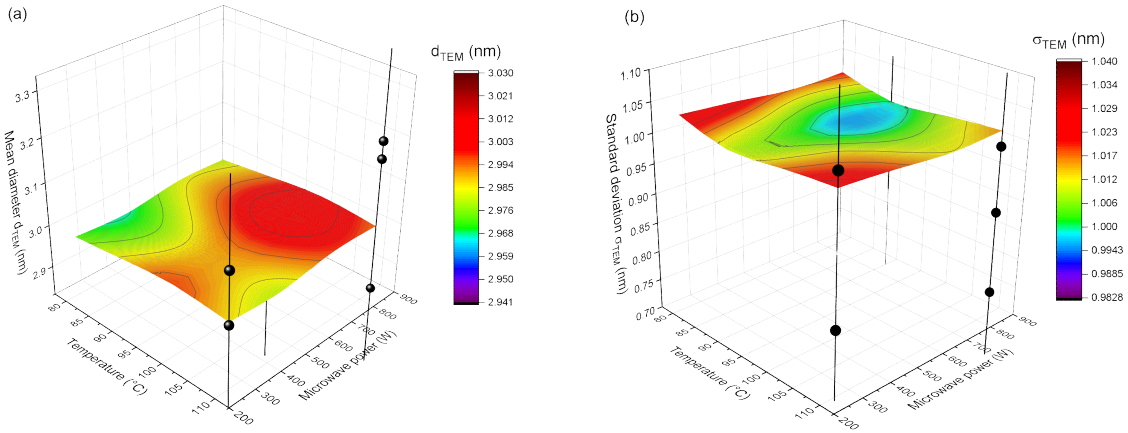

Figure 8: surface response plot of the ED for the effect of the temperature (factor B) and for the microwave power (factor D) on the mean diameter d_{TEM} (a) and on the standard deviation σ_{TEM} (b) with the experiments (spherical) with their sd to validate the ED.

3. Conclusion

Superparamagnetic iron oxide nanoparticles (SPIONs) were synthesized by a derivate coprecipitation method with a microwave process. However, this method is not well developed, an experimental design was therefore carried out to determine the best microwave parameters to synthesise SPIONs. Indeed, without an experimental design, many experiments should have been synthesised: different factors (ramp time, temperature, stage time, microwave power and moment of stirring) has been choose at different values (levels) in order to obtain responses from the characterizations. Thus, a number of 1024 experiments has been reduced to 16 experiments.
In general, the size of these SPIONs is between 2.68 nm and 3.57 nm with a standard deviation between 0.83 nm to 1.32 nm. The other responses confirm that the inorganic core is magnetite with a slight oxidation (sub stoichiometric magnetite $Fe_{3-\delta}O_4$) with a superparamagnetic behaviour. Then, thanks to the repetition of this experimental design three times by a same operator and one time by another operator, the reproducibility and the repeatability has been confirmed with the statistical tests (ANOVA). Finally, a simulation of this experimental design is carried out and allowed to obtain the responses of the 1024 experiments: a surface response is obtained with the different factor for each response. To validate this experimental design, some experiments (selected for their responses and randomly selected) are carried out and the different responses are near to the theoretical values. However, when the percentage of ligands is not between 30% and 35%, a wide fluctuation in values is observed. To avoid these variations, a better control of the washing should be achieved to obtain superparamagnetic iron oxide nanoparticles with the best properties for MRI applications.

4. Materials and methods

4.1. Materials

Ferric chloride ($FeCl_3.6H_2O$) and ferrous chloride ($FeCl_2.4H_2O$) were purchased from Alfa Aeser, citric acid ($C_6H_8O_7$), absolute ethanol and ammonium hydroxide (NH_4OH) were purchased from Sigma Aldrich. In all experiments, ultrapure water (resistivity = 18.2 MΩ.cm) was used.

4.2. Synthesis

For all experiment, the chemical conditions were fixed in order to see the influence of microwave parameters on the SPIONs synthesis. A solution of ferrous chloride ($FeCl_2.4H_2O$, 5.03 mmol), ferric chloride ($FeCl_3.6H_2O$, 3.70 mmol) and citric acid ($C_6H_8O_7$, 3.16 mmol) were mixed in ultrapure water in a Pirex reactor for microwave. Then, 5 mL of ammonium hydroxide (NH_4OH) is added to generate the precipitation of iron ions: the solution turns brown to black. The reactor is placed directly in the microwave. The microwave is a single mode microwave from Anton Paar (Monowave 400) which operates at a frequency of 2.45 GHz and with a maximum power of 850 W.
After heating, the solution is collected and washed several times to remove parasitic ions. For this, a first washing step is carried out with a mixture of absolute ethanol and nanoparticle solution. This mixture is centrifugated during 5 min at 10 000 rpm. After the centrifugation, SPIONs are collected and redispersed in a few volumes of ultrapure water. After an adding of absolute ethanol, the mixture is centrifugated another time at 10 000 rpm during 5 min. Finally, after this second stage, SPIONs are collected, and a part is dried in an oven at 80°C and another part is dispersed in water. The powder obtain after the drying is used for certain techniques and

the SPIONs in the liquid state allow to see the stability of the nanoparticles in an aqueous media and for certain techniques too.

4.3. Characterizations techniques

4.3.1. Transmission Electron Microscopy

Transmission Electron Microscopy (TEM) is carried out to determine the size, the size distribution, and the shape of nanoparticles. TEM is a CM200-FEI working at 200 kV (point resolution 0.27 nm). To visualize SPIONs, a drop of the solution is placed on a copper grid with a carbon film and dried to remove the solvent. After the analysis, the size distribution as well as the mean diameter of SPIONs is calculated using free software ImageJ.

4.3.2. Dynamic Light Scattering

Dynamic Light Scattering (DLS) was performed by the ZETASIZER Nano ZS device from Malvern Instrumental. The SPIONs solution was diluted to obtain a mass concentration of 0.2 $mg.mL^{-1}$. With this characterization, the stability as well as the hydrodynamic diameter are determined. DLS measurements are performed three times and the average of these three measurements will be presented in this study. In addition, the number measure was kept to allow a comparison between the hydrodynamic diameter and the diameter obtain by TEM measurement.[53]

4.3.3. X-Ray Diffraction

X-Ray Diffraction (XRD) patterns were recorded at room temperature with an INEL CPS120 equipped with a monochromatic cobalt radiation (Co Kα = 0.17886 nm) at grazing angle of incidence simultaneously at 120°.

4.3.4 Fourier Transform Infra-Red

Fourier Transform Infra-Red spectroscopy (FTIR) was performed with a Nicolet 6700 from Thermo-Fischer between 400 and 4 000 cm^{-1}.

4.3.5. Thermogravimetric measurements

Thermogravimetric analysis (TGA) was performed to determine the mass percentage of ligands (citrate) and of iron oxide. A SETSSYS EV 1750 TGA microbalance from Setaram. Experiments are carried out in the temperature range of 20 to 600°C under air flow (20 $mL.min^{-1}$) at a heating rate of 10°C/min.

4.3.6. Magnetic measurements

A Superconducting Quantum Interference Device (SQUID equipped with a Vibrating Sample Magnetometer (VSM) are performed to determine the magnetic state, the magnetization saturation (M_S); The magnetic field applied for these characterizations is sweeping from +50 000 to -50 000 Tesla and then -50 000 Oe to +50 000 Oe. Then, to determine the blocking temperature (T_B), a Zero Field Cooled – Field Cooled (ZFC-FC) curve is carried out. The sample was cooled to 5K without a magnetic field. At 5K, a low magnetic field (200 Oe) is applied, and the temperature is increased to 300K (ZFC curve). Finally, the sample is cooled another time to 5K but with an applied magnetic field, the same during the heating from 5K to 300K: this curve is the FC curve.

4.4. Experimental Design (ED)

The goal of this work is to determine the influence of microwave parameters on the SPIONs synthesis. The SPIONs synthesis is composed of three steps: the first is a temperature ramp

(called t_1), the second a temperature tray (called t_2) and finally a decrease of the temperature to room temperature (called t_3). Five parameters have been chosen to see their influence on the physico-chemical parameters of SPIONs: the time of the ramp (called A), the temperature of the synthesis (called B), the time of the stage (called C), the microwave power (called D) and the moment of stirring (called E). For each microwave parameters, four levels (from 1 to 4) have been defined and are summarized on **Table 2**.

Table 2: factor levels of each microwave parameters.

Variable parameters	Level			
	1	2	3	4
A: ramp time	5 min	10 min	15 min	20 min
B: temperature	80°C	90°C	100°C	110°C
C: stage time	10 min	20 min	30 min	40 min
D: microwave power	250 W	450 W	650 W	850 W
E: moment of stirring	Without	t_1	t_2	t_3

There are therefore five parameters with four levels: the number of experiments is equal to 4^5 experiments or 1024 experiments. In order to examine all microwaves parameters and their influences on the SPIONs synthesis, a reduction of the synthesis number is mandatory. For this, statistical tables established by Tagushi during the middle of 20th century are used. It exists several tables with different number of factors and levels.[54] For our study, a table where all levels of each parameter are equally represented has been choose: the table is a $L_{16}(4^5)$. The construction of the table is described on **Figure S1**. The number of experiments is reduced from 1024 to 16. For the next of this study, each simple will name S1 to S16. The microwave parameters of each sample are described on **Table S1**.

To show the influence of these parameters, a study of the response and after a simulation of these results are carried out: surface responses are realized to determine the best conditions for microwave parameters to synthesize and to use SPIONs as CA. The different responses are the mean diameter (d_{TEM}), the standard deviation of the diameter (σ_{TEM}), the hydrodynamic diameter (d_{DLS}), the lattice parameter (a_{XRD}), the crystallite size (t_{XRD}), the percentage of ligands ($\%_{lig}$), the magnetization saturation at 300K (M_{s_300K}) and at 5K (M_{s_5K}) and the blocking temperature (T_B). The ED has been carried out four times to show the reproducibility and the repeatability. For the repeatability, the ED has reproduced three times by the same operator in the same conditions. The samples from this ED are named SX_{yA} with X the number of the sample from the ED (from 1 to 16), y the number of the repetition of the DE (y = 1;2;3) and A the operator. For the reproducibility, the ED has realized by another operator in the same conditions. The sample from this ED are named SX_{1B} with X the number of the sample from the ED and B the second operator. A total of 64 experiments for this study are therefore realized and the average of responses of the same experiments are allowed to simulate the 1024 experiments. The 64 samples are summarized on **Table S2**.

Finally, with this simulation, a surface response in function of the microwave parameters is obtained. To validate the ED, three randomly experiments within the range of the factors and three selected experiments are shown on the surface response.

Acknowledgements

The authors knowledge the center of Microscopy, X-Gamma, Optic and Magnetism of Institute Jean Lamour.

References

[1] J. Peng, W. Zhang, L. Chen, T. Wu, M. Zheng, H. Dong, H. Hu, Y. Xiao, Y. Liu and Y. Liang, *Chemical Engineering Journal*, **2021**, 404, 126461.

[2] M. Valvo, C. Floraki, E. Paillard, K. Edström and D. Vernardou, *Nanomaterials*, **2022**, 12, 1436.

[3] M. G. Montiel Schneider, M. J. Martín, J. Otarola, E. Vakarelska, V. Simeonov, V. Lassalle and M. Nedyalkova, *Pharmaceutics*, **2022**, 14, 204.

[4] M.-A. Karageorgou, P. Bouziotis, E. Stiliaris and D. Stamopoulos, *Nanomaterials*, **2023**, 13, 503.

[5] E. A. Vermeij, M. I. Koenders, M. B. Bennink, L. A. Crowe, L. Maurizi, J.-P. Vallée, H. Hofmann, W. B. van den Berg, P. L. E. M. van Lent and F. A. J. van de Loo, *PLoS ONE*, **2015**, 10, e0126687.

[6] Z. Nemati, J. Alonso, I. Rodrigo, R. Das, E. Garaio, J. Á. García, I. Orue, M.-H. Phan and H. Srikanth, *J. Phys. Chem. C*, **2018**, 122, 2367–2381.

[7] J. M. Paez-Muñoz, F. Gámez, Y. Fernández-Afonso, R. Gallardo, M. Pernia Leal, L. Gutiérrez, J. M. De La Fuente, C. Caro and M. L. García-Martín, *J. Mater. Chem. B*, **2023**, 11, 11110–11120.

[8] M. Soleymani, M. Velashjerdi, Z. Shaterabadi and A. Barati, *Carbohydrate polymers*, **2020**, 237, 116130.

[9] L. Chen, Y. Wu, H. Wu, J. Li, J. Xie, F. Zang, M. Ma, N. Gu and Y. Zhang, *Acta Biomaterialia*, **2019**, 96, 491–504.

[10] A. Nicolae-Maranciuc, D. Chicea and L. M. Chicea, *International Journal of Molecular Sciences*, **2022**, 23, 5778.

[11] W.-C. Ko, S.-J. Wang, C.-Y. Hsiao, C.-T. Hung, Y.-J. Hsu, D.-C. Chang and C.-F. Hung, *Molecules*, **2022**, 27, 1551.

[12] J. H. Jin, H. Um, J. H. Oh, Y. Huh, Y. Jung and D. Kim, *Materials Chemistry and Physics*, **2022**, 287, 126345.

[13] S. Laurent, D. Forge, M. Port, A. Roch, C. Robic, L. Vander Elst and R. N. Muller, *Chem. Rev.*, **2008**, 108, 2064–2110.

[14] H. Shokrollahi, *Materials Science and Engineering: C*, **2013**, 33, 4485–4497.

[15] M.-A. Fortin, in *Magnetic Characterization Techniques for Nanomaterials*, ed. C. S. S. R. Kumar, Springer Berlin Heidelberg, Berlin, Heidelberg, **2017**, pp. 511–555.

[16] C. H. Evans, *Biochemistry of the Lanthanides*, Springer Science & Business Media, **2013**, vol. 8.

[17] J. B. Lansman, *The Journal of general physiology*, **1990**, 95, 679–696.

[18] L. Zhang, R. Liu, H. Peng, P. Li, Z. Xu and A. K. Whittaker, *Nanoscale*, **2016**, 8, 10491–10510.

[19] G. Wang, X. Zhang, A. Skallberg, Y. Liu, Z. Hu, X. Mei and K. Uvdal, *Nanoscale*, **2014**, 6, 2953.

[20] S. Laurent, L. V. Elst and R. N. Muller, in *The Chemistry of Contrast Agents in Medical Magnetic Resonance Imaging*, eds. A. Merbach, L. Helm and É. Tóth, John Wiley & Sons, Ltd, Chichester, UK, **2013**, pp. 427–447.

[21] J. L. Dormann, *Advances in Chemical Physics*, **1997**, 98, 283–494.

[22] C. Chen, J. Ge, Y. Gao, L. Chen, J. Cui, J. Zeng and M. Gao, *WIREs Nanomed Nanobiotechnol*, **2022**, 14, e1740.

[23] N. Tabassum, V. Singh, V. K. Chaturvedi, E. Vamanu and M. P. Singh, *Pharmaceutics*, **2023**, 15, 1726.

[24] S. Slimani, C. Meneghini, M. Abdolrahimi, A. Talone, J. P. M. Murillo, G. Barucca, N. Yaacoub, P. Imperatori, E. Illés, M. Smari, E. Dhahri and D. Peddis, *Applied Sciences*, **2021**, 11, 5433.

[25] M. O. Besenhard, L. Panariello, C. Kiefer, A. P. LaGrow, L. Storozhuk, F. Perton, S. Begin, D. Mertz, N. T. K. Thanh and A. Gavriilidis, *Nanoscale*, **2021**, 13, 8795–8805.
[26] P. Cheah, T. Cowan, R. Zhang, A. Fatemi-Ardekani, Y. Liu, J. Zheng, F. Han, Y. Li, D. Cao and Y. Zhao, *Nanoscale*, **2020**, 12, 9272–9283.
[27] Y. Bao, J. A. Sherwood and Z. Sun, *J. Mater. Chem. C*, **2018**, 6, 1280–1290.
[28] G. Thomas, F. Demoisson, J. Boudon and N. Millot, *Dalton Trans.*, **2016**, 45, 10821–10829.
[29] H. Kahil, A. Faramawy, H. El-Sayed and A. Abdel-Sattar, *Crystals*, **2021**, 11, 1153.
[30] I.-C. Masthoff, M. Kraken, D. Mauch, D. Menzel, J. A. Munevar, E. Baggio Saitovitch, F. J. Litterst and G. Garnweitner, *J Mater Sci*, **2014**, 49, 4705–4714.
[31] Q. Wang, X. Ma, H. Liao, Z. Liang, F. Li, J. Tian and D. Ling, *ACS Nano*, **2020**, 14, 2053–2062.
[32] C. Xu and S. Sun, *Advanced Drug Delivery Reviews*, **2013**, 65, 732–743.
[33] S. Masur, B. Zingsem, T. Marzi, R. Meckenstock and M. Farle, *Journal of Magnetism and Magnetic Materials*, **2016**, 415, 8–12.
[34] C. Goroncy, P. E. J. Saloga, M. Gruner, M. Schmudde, J. Vonnemann, E. Otero, R. Haag and C. Graf, *Zeitschrift für Physikalische Chemie*, **2018**, 232, 819–844.
[35] R. K. Kottana, L. Maurizi, B. Schnoor, K. Morris, J. A. Webb, M. A. Massiah, N. Millot and A. Papa, *Small*, **2021**, 17, 2004945.
[36] K. Jani, N. Kaushal, M. Sadoqi, G. Long, Z.-S. Chen and E. Squillante, *Journal of Magnetism and Magnetic Materials*, **2021**, 533, 167970.
[37] F. M. E. Segers, A. V. Ruder, M. M. Westra, T. Lammers, S. M. Dadfar, K. Roemhild, T. S. Lam, M. E. Kooi, K. B. J. M. Cleutjens, F. K. Verheyen, G. W. H. Schurink, G. R. Haenen, T. J. C. van Berkel, I. Bot, B. Halvorsen, J. C. Sluimer and E. A. L. Biessen, *Cardiovascular Research*, **2022**, cvac032.
[38] A. Sathya, S. Kalyani, S. Ranoo and J. Philip, *Journal of Magnetism and Magnetic Materials*, **2017**, 439, 107–113.
[39] Y.-J. Liang, Y. Zhang, Z. Guo, J. Xie, T. Bai, J. Zou and N. Gu, *Chem. Eur. J.*, **2016**, 22, 11807–11815.
[40] J.-S. Schanche, *Mol Divers*, **2003**, 7, 291–298.
[41] M. E. F. Brollo, S. Veintemillas-Verdaguer, C. M. Salván and M. del P. Morales, *Contrast Media & Molecular Imaging*, **2017**, 2017, 1–13.
[42] H.-C. Roth, S. P. Schwaminger, M. Schindler, F. E. Wagner and S. Berensmeier, *Journal of Magnetism and Magnetic Materials*, **2015**, 377, 81–89.
[43] T. M. Laid, K. Abdelhamid, L. S. Eddine and B. Abderrhmane, *Journal of Molecular Structure*, **2021**, 1229, 129497.
[44] B. H. Hui and M. N. Salimi, *IOP Conf. Ser.: Mater. Sci. Eng.*, **2020**, 743, 012036.
[45] M. Mahmoudi, A. Simchi, M. Imani, A. S. Milani and P. Stroeve, *J. Phys. Chem. B*, **2008**, 112, 14470–14481.
[46] T. Girardet, A. Cherraj, A. Pinzano, C. Henrionnet, F. Cleymand and S. Fleutot, *Pure and Applied Chemistry*, **2021**, 93, 1265–1273.
[47] N. Ohannesian, C. T. De Leo and K. S. Martirosyan, *Materials Today: Proceedings*, **2019**, 13, 397–403.
[48] A. M. Predescu, E. Matei, A. C. Berbecaru, C. Pantilimon, C. Drăgan, R. Vidu, C. Predescu and V. Kuncser, *R. Soc. open sci.*, **2018**, 5, 171525.
[49] Y. Sahoo, A. Goodarzi, M. T. Swihart, T. Y. Ohulchanskyy, N. Kaur, E. P. Furlani and P. N. Prasad, *J. Phys. Chem. B*, **2005**, 109, 3879–3885.
[50] F. Malega, I. P. T. Indrayana and E. Suharyadi, *JIPFAlBiruni*, **2018**, 7, 129–138.
[51] P. Roushenas, Z. Yusop, Z. Majidnia and R. Nasrollahpour, *Desalination and Water Treatment*, **2016**, 57, 5837–5841.

[52] I. J. Bruvera, P. Mendoza Zélis, M. Pilar Calatayud, G. F. Goya and F. H. Sánchez, *Journal of Applied Physics*, **2015**, 118, 184304.
[53] J. Lim, S. P. Yeap, H. X. Che and S. C. Low, *Nanoscale Res Lett*, **2013**, 8, 381.
[54] A. A. Dar and N. Anuradha, *International Journal of Services, Economics and Management*, **2020**, 11, 1–20.

Supporting Information

One step superparamagnetic iron oxide nanoparticles by a microwave process: optimization of microwave parameters with an experimental design

*Thomas Girardet, Morgane Kessler, Sylvie Migot, Lionel Aranda, Sébastien Diliberto, Stéphane Suire, Tom Ferté, Sébastien Hupont, Franck Cleymand, Solenne Fleutot**

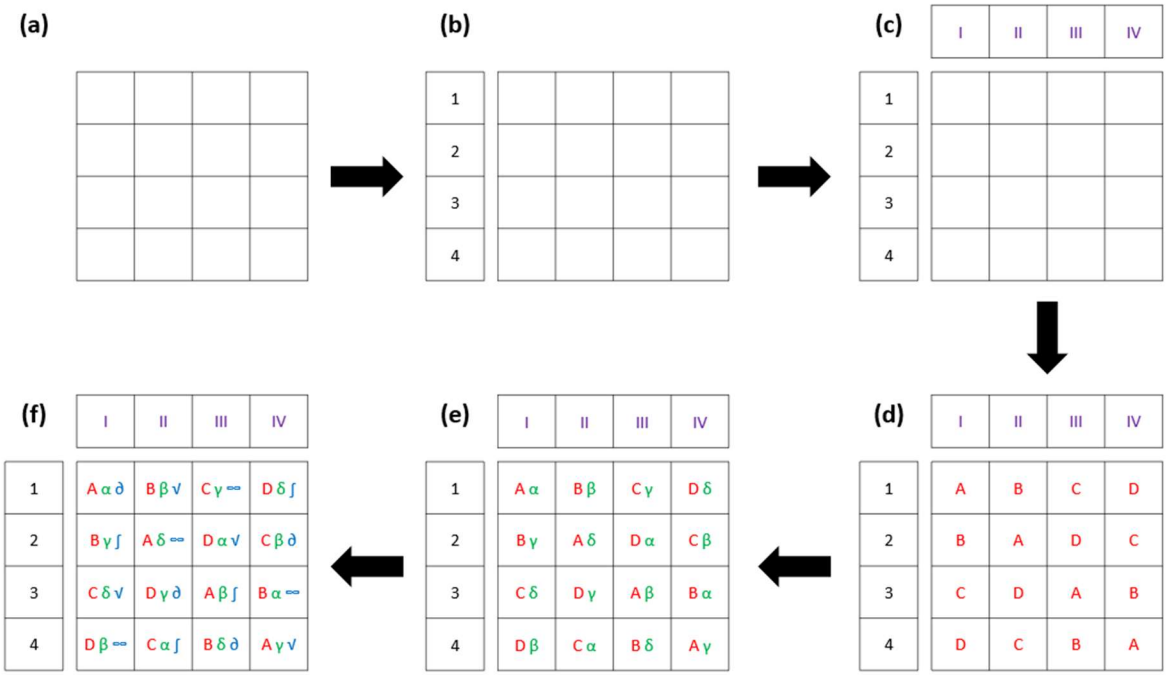

Figure S1: steps on the construction of the experimental design. One square corresponds to an experiment (a). Each line corresponds to a level of the factor A (b) and each column correspond to a level of the factor B (c). Then, for factors C, D and E (respectively (d), (e) and (f)), each level is present on one column and one line.

Table S1: table of the microwave parameters for the different samples. The highlighted parameters are the synthesis described on the publication.

Sample	A (time of the ramp in min)	B (temperature in °C)	C (time of the stage in min)	D (microwave power in W)	E (moment of the stirring)
S1	1 (5 min)	1 (80 °C)	1 (10 min)	1 (250 W)	1 (without)
S2	1 (5 min)	2 (90 °C)	2 (20 min)	2 (450 W)	2 (t_1)
S3	1 (5 min)	3 (100 °C)	3 (30 min)	3 (650 W)	3 (t_2)
S4	1 (5 min)	4 (110 °C)	4 (40 min)	4 (850 W)	4 (t_3)
S5	2 (10 min)	1 (80 °C)	2 (20 min)	3 (650 W)	4 (t_3)
S6	2 (10 min)	2 (90 °C)	1 (10 min)	4 (850 W)	3 (t_2)
S7	2 (10 min)	3 (100 °C)	4 (40 min)	1 (250 W)	2 (t_1)
S8	2 (10 min)	4 (110 °C)	3 (30 min)	2 (450 W)	1 (without)
S9	3 (15 min)	1 (80 °C)	3 (30 min)	4 (850 W)	2 (t_1)
S10	3 (15 min)	2 (90 °C)	4 (40 min)	3 (650 W)	1 (without)
S11	3 (15 min)	3 (100 °C)	1 (10 min)	2 (450 W)	4 (t_3)
S12	3 (15 min)	4 (110 °C)	2 (20 min)	1 (250 W)	3 (t_2)
S13	4 (20 min)	1 (80 °C)	4 (40 min)	2 (450 W)	3 (t_2)
S14	4 (20 min)	2 (90 °C)	3 (30 min)	1 (250 W)	4 (t_3)
S15	4 (20 min)	3 (100 °C)	2 (20 min)	4 (850 W)	1 (without)
S16	4 (20 min)	4 (110 °C)	1 (10 min)	3 (650 W)	2 (t_1)

Table S2: summarize of all samples of the experimental design. The values in bold are described on the supplementary information. The values crossed out are removed on the simulation due to the Dixon's test. The value highlighted is described on the publication.

Sample	d_{TEM} (nm)	σ_{TEM} (nm)	d_{hydro} (nm)	a_{XRD} (Å)	t_{XRD} (nm)	$\%_{lig}$ (%)	M_s 300K (emu.g^{-1})	M_s 5K (emu.g^{-1})	T_B (K)
$S1_{1A}$	2.91	1.02	6.91	8.401	3.33	~~34~~	43.08	69.85	12
$S1_{2A}$	2.83	1.10	8.30	8.408	3.29	26	36.39	57.85	15
$S1_{3A}$	2.92	1.12	7.88	8.362	3.44	26	49.85	69.07	19
$S1_{1B}$	2.95	1.08	9.92	8.391	3.87	26	49.24	70.96	24
$S2_{1A}$	2.82	0.83	6.50	8.393	3.89	33	32.47	56.89	14
$S2_{2A}$	3.08	1.08	10.00	8.391	3.62	32	51.09	72.95	13
$S2_{3A}$	2.97	1.00	8.56	~~8.354~~	3.46	28	55.52	75.01	14
$S2_{1B}$	3.05	0.88	6.10	8.391	3.37	24	58.37	78.99	~~44~~
$S3_{1A}$	2.95	0.89	8.17	8.404	3.72	35	52.71	78.11	15
$S3_{2A}$	3.16	1.09	9.74	8.382	3.60	16	60.28	74.74	34
$S3_{3A}$	3.57	1.02	8.91	8.359	3.85	35	54.47	77.00	13
$S3_{1B}$	3.18	0.81	7.82	8.391	3.55	25	58.18	77.60	24
$S4_{1A}$	3.37	1.05	7.71	8.394	4.02	37	51.87	73.45	15
$S4_{2A}$	2.98	1.04	6.50	8.375	3.56	29	51.86	72.20	14
$S4_{3A}$	3.22	0.94	8.84	8.350	3.70	25	59.48	76.74	17
$S4_{1B}$	**3.07**	**0.83**	**7.38**	**8.393**	**3.86**	**20**	**59.95**	**78.46**	~~43~~
$S5_{1A}$	3.02	0.96	5.61	8.399	3.65	32	29.09	48.58	12
$S5_{2A}$	2.68	0.97	9.56	8.369	3.50	34	46.16	65.26	14
$S5_{3A}$	3.17	1.26	9.29	8.374	3.80	39	49.35	64.71	12
$S5_{1B}$	2.88	1.00	7.39	8.386	3.34	31	50.06	76.99	16
$S6_{1A}$	3.13	0.96	8.11	8.390	3.32	27	49.69	69.25	17
$S6_{2A}$	2.88	0.92	6.12	8.432	3.02	35	~~23.86~~	45.01	11
$S6_{3A}$	2.97	0.91	8.45	8.357	3.51	35	48.15	71.87	13
$S6_{1B}$	3.22	0.99	6.87	8.387	3.20	32	48.39	55.00	13
$S7_{1A}$	**3.48**	**1.17**	**7.32**	**8.394**	**3.54**	**31**	**51.01**	**72.13**	**14**
$S7_{2A}$	3.16	1.19	7.63	8.405	3.58	20	64.52	80.99	25
$S7_{3A}$	3.08	0.92	7.68	8.353	3.62	27	57.12	75.78	16
$S7_{1B}$	3.06	0.84	5.98	8.392	3.47	25	61.40	83.10	20
$S8_{1A}$	3.11	0.92	11.70	8.400	3.86	17	58.81	75.38	46
$S8_{2A}$	3.21	1.18	8.94	8.393	3.63	35	55.31	77.30	13
$S8_{3A}$	3.13	1.16	7.54	8.362	3.93	36	53.04	75.40	14
$S8_{1B}$	2.68	1.02	26.53	8.377	3.94	22	64.73	86.30	25
$S9_{1A}$	3.22	1.17	7.50	8.391	3.93	32	47.20	72.83	14
$S9_{2A}$	2.93	1.00	5.71	8.391	3.52	23	57.05	76.23	20
$S9_{3A}$	3.09	1.32	12.91	8.386	3.69	37	49.90	73.44	13
$S9_{1B}$	2.88	0.99	6.24	8.370	3.42	32	50.97	75.66	15
$S10_{1A}$	3.21	~~1.22~~	8.63	8.391	3.61	35	57.48	79.13	17
$S10_{2A}$	3.19	0.88	8.11	8.398	3.69	37	53.78	76.68	12
$S10_{3A}$	3.00	0.86	6.65	8.379	3.50	36	55.04	76.86	13
$S10_{1B}$	2.74	0.87	6.76	8.377	3.50	27	59.14	77.61	22
$S11_{1A}$	2.96	1.12	13.54	8.393	4.43	39	17.49	42.77	10

$S11_{2A}$	3.03	1.17	10.69	8.393	-----	32	59.85	73.50	16
$S11_{3A}$	3.16	0.92	7.34	8.378	3.64	36	51.96	72.78	12
$S11_{1B}$	2.95	0.86	6.57	8.384	3.68	25	59.14	83.76	20
$S12_{1A}$	3.17	1.30	9.10	8.384	3.47	34	55.23	71.19	15
$S12_{2A}$	2.92	0.96	8.51	8.408	3.57	31	49.78	69.96	15
$S12_{3A}$	3.15	1.14	6.48	8.374	3.62	37	44.57	66.86	11
$S12_{1B}$	2.82	0.98	6.76	8.376	3.69	24	64.11	85.36	23
$S13_{1A}$	3.30	0.87	8.93	8.390	3.99	36	46.02	70.66	12
$S13_{2A}$	3.06	1.13	7.83	8.366	3.58	30	54.07	74.38	15
$S13_{3A}$	2.93	1.18	8.68	8.379	3.67	33	52.93	74.11	15
$S13_{1B}$	2.89	1.02	8.27	8.378	3.98	33	56.84	94.62	17
$S14_{1A}$	2.87	1.11	6.74	8.391	3.88	35	43.12	64.52	12
$S14_{2A}$	**3.11**	**0.99**	**9.62**	**8.368**	**3.59**	**35**	**53.07**	**76.81**	**12**
$S14_{3A}$	2.91	0.86	8.03	8.362	3.62	35	51.07	71.73	13
$S14_{1B}$	2.93	1.10	7.81	8.377	3.21	37	44.77	69.00	11
$S15_{1A}$	3.06	1.09	7.59	8.389	3.93	34	59.84	80.76	13
$S15_{2A}$	3.14	1.07	8.81	8.390	3.70	23	63.54	80.11	20
$S15_{3A}$	3.00	0.85	7.23	~~8.366~~	3.66	35	55.62	77.18	13
$S15_{1B}$	2.79	0.88	9.64	8.388	3.60	22	62.15	66.98	21
$S16_{1A}$	3.21	1.12	6.95	8.395	3.78	35	49.35	72.12	11
$S16_{2A}$	2.94	0.84	7.82	8.354	3.55	38	62.73	87.73	14
$S16_{3A}$	3.21	1.24	9.74	8.378	3.28	30	52.03	72.27	13
$S16_{1B}$	3.01	0.94	7.65	8.378	3.75	36	54.43	60.33	14

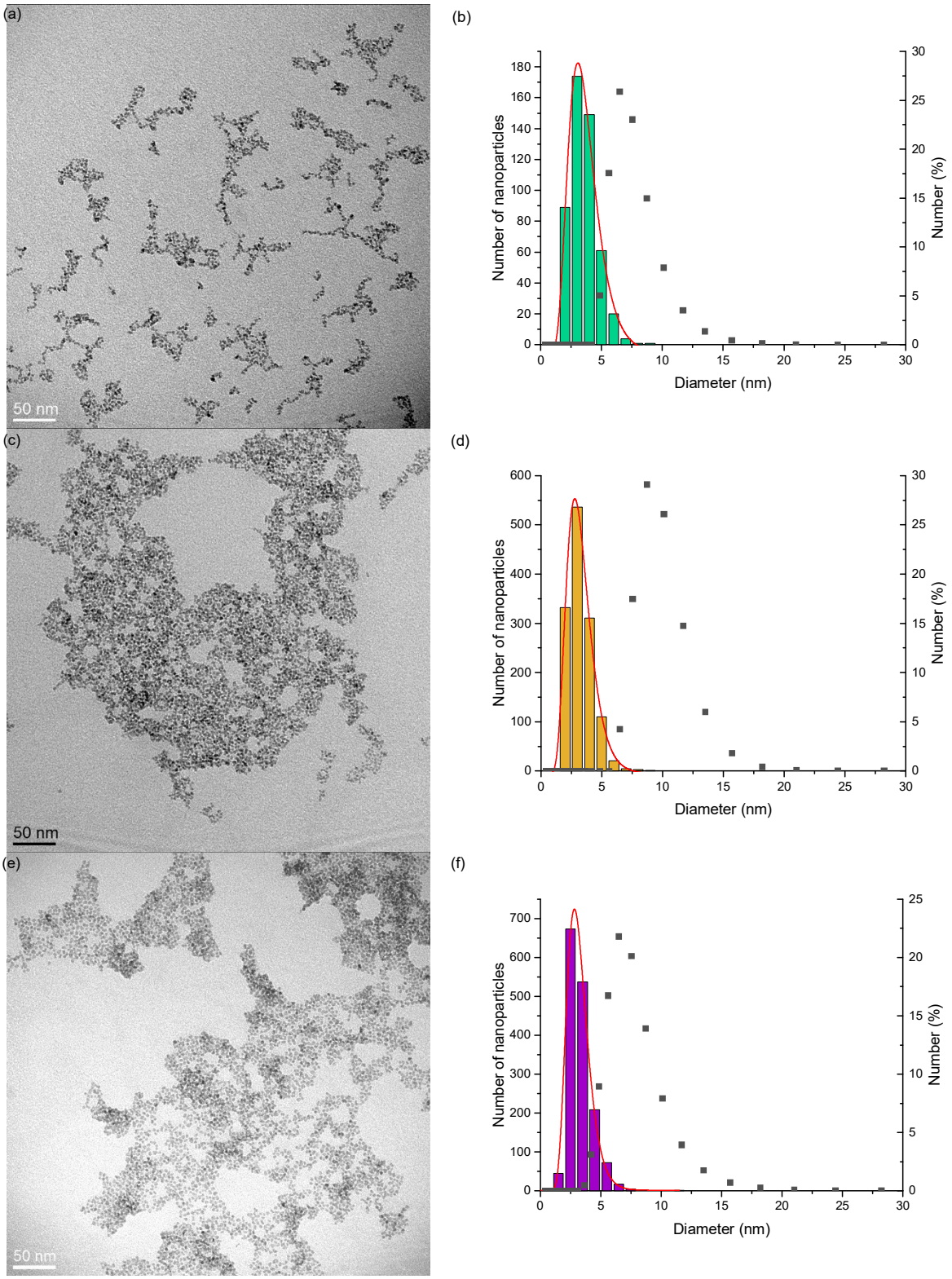

Figure S2: TEM images of $S7_{1A}$ (a), $S14_{2A}$ (c) and $S4_{1B}$ (e) with their respectively size distributions (b), (d) and (f). The main diameter of $S7_{1A}$ is 3.48 ± 1.17 nm of $S14_{2A}$ is 3.11 ± 0.99 nm and of 3.07 ± 0.83 nm. In each graph, the DLS measurements (symbols) is represented to determine the hydrodynamic diameter. This value is equal to 7.32 nm (b), 9.62 nm (d) and 7.38 nm (f) respectively for $S7_{1A}$, $S14_{2A}$ and $S4_{1B}$.

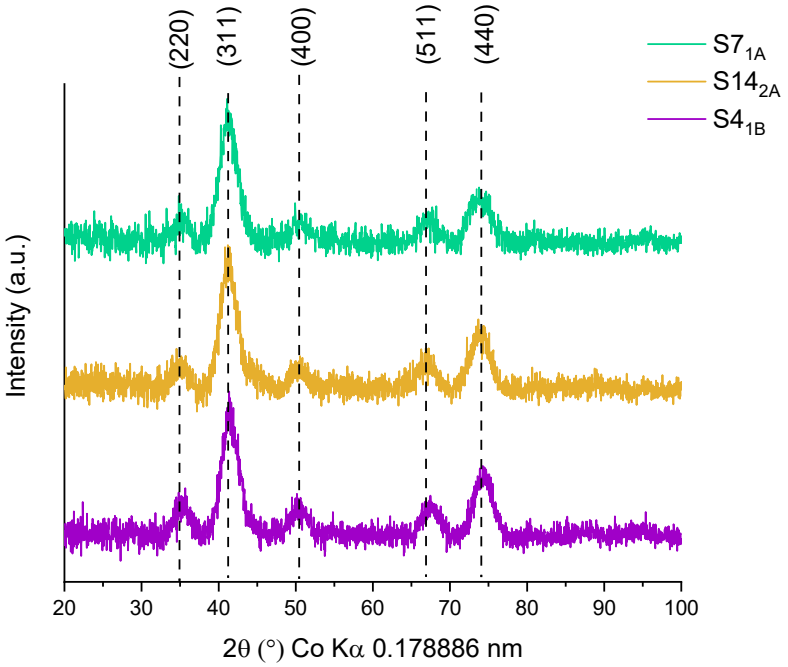

Figure S3: XRD patterns of $S7_{1A}$ (green), $S14_{2A}$ (orange) and $S4_{1B}$ (purple) with the plans of the spinel structure of magnetite Fe_3O_4.

Debye-Scherrer equation:

$$t = \frac{k \times \lambda}{\sqrt{H^2 - s^2} \times \cos(\theta)}$$

With t the crystallite size (nm), λ the wavelength (λ= 0.178886 nm), k a correction factor (0.9), H the FWHM of the main peak (311) in radian, s the FWHM of a main peak of a Si reference (s = 0.323°) and θ the position of the main peak (°)

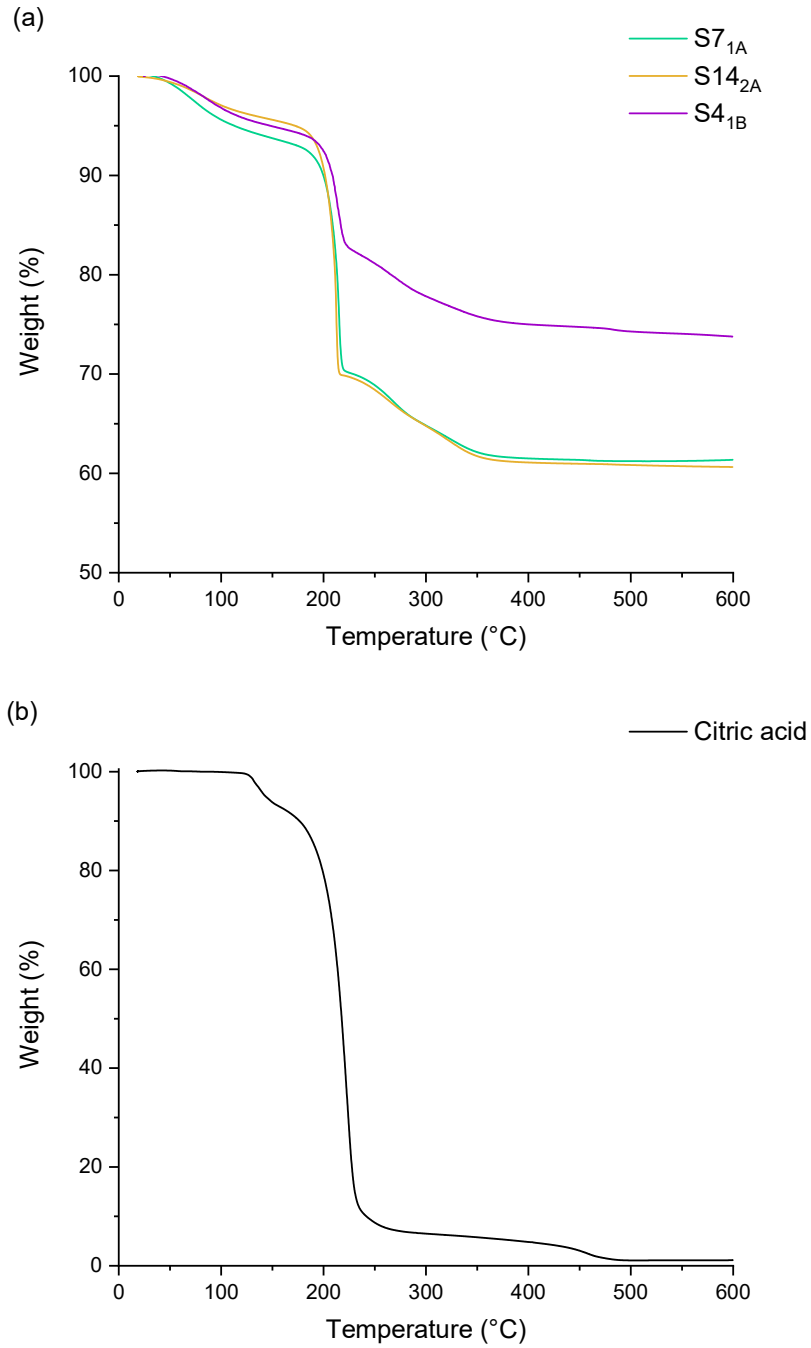

Figure S4: TGA curves of $S7_{1A}$ (green), $S14_{2A}$ (orange) and $S4_{1B}$ (purple) from 20°C to 600°C (a) and of pure citric acid (b).

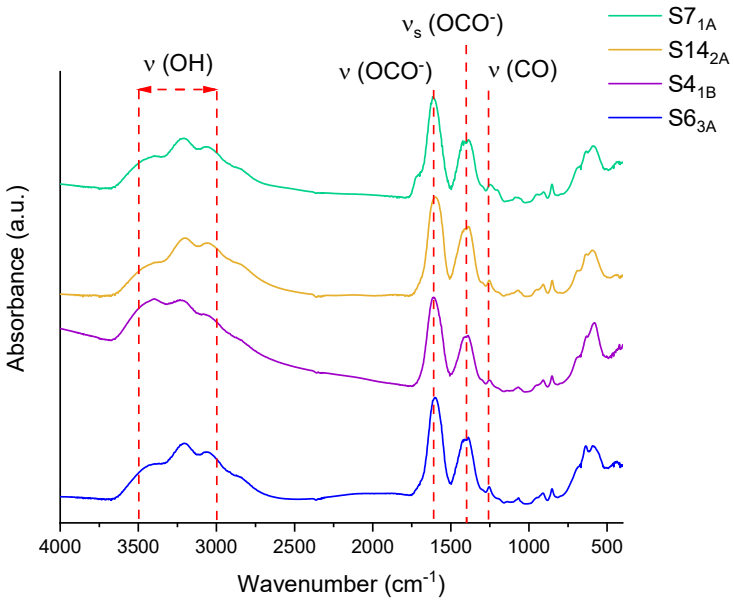

Figure S5: FTIR spectra of $S7_{1A}$ (green), $S14_{2A}$ (orange), $S4_{1B}$ (purple) and $S6_{3A}$ (blue) with the vibrational bands of citrate to confirm this ligand around the iron oxide core.

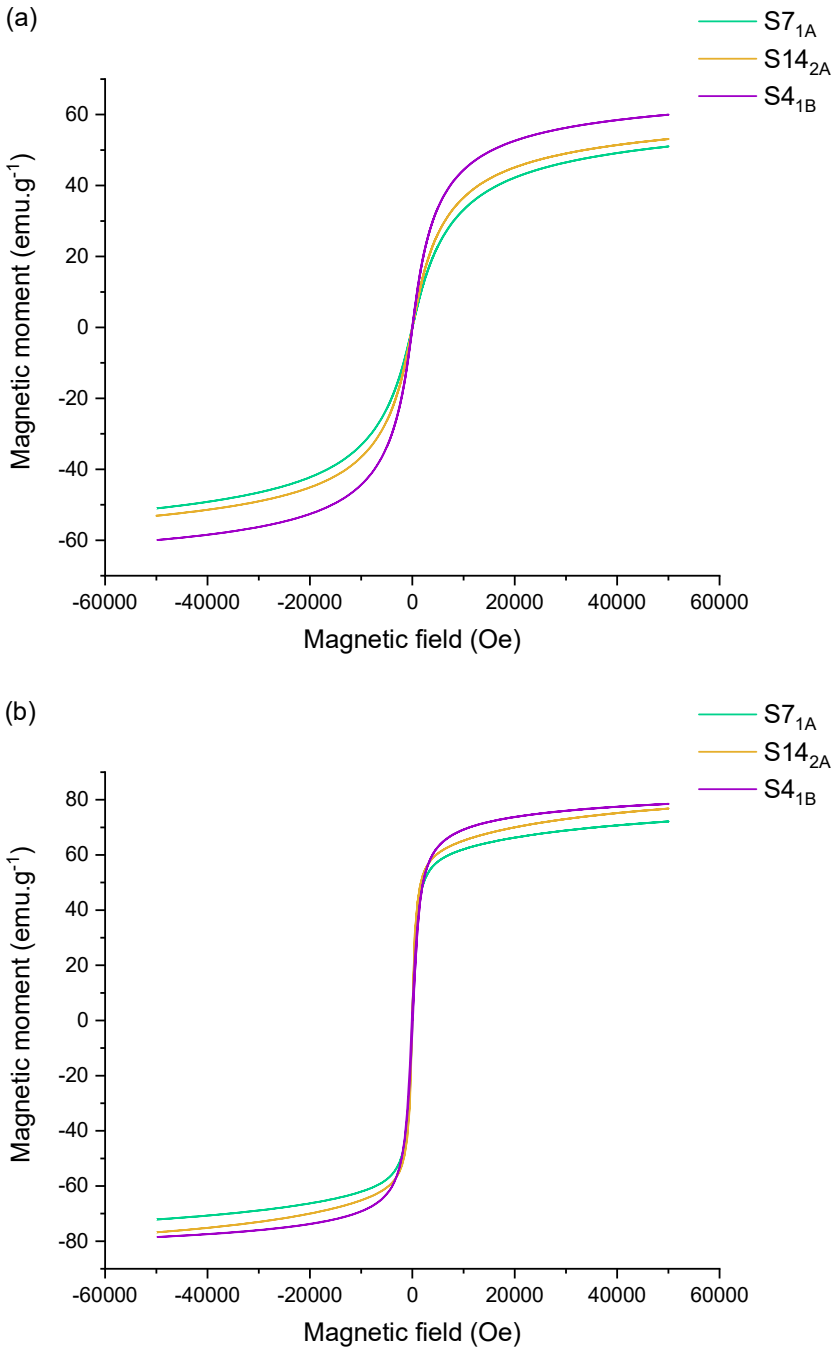

Figure S6: magnetic cycles of $S7_{1A}$ (green), $S14_{2A}$ (orange) and $S4_{1B}$ (purple) at 300K (a) and at 5K (b).

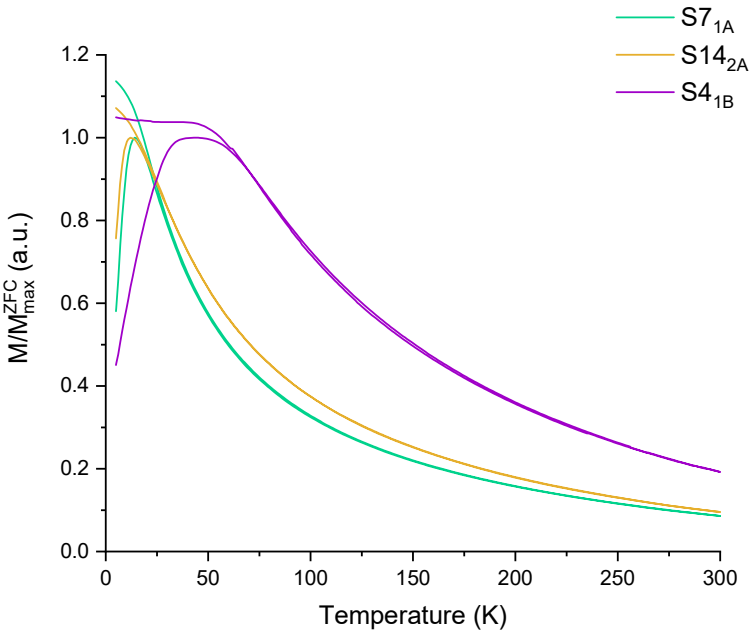

Figure S7: ZFC-FC curve of $S7_{1A}$ (green), $S14_{2A}$ (orange) and $S4_{1B}$ (purple) with a blocking temperature equals to 14K, 12K and 43K respectively for $S7_{1A}$, $S14_{2A}$ and $S4_{1B}$.

Figure S8: Dixon's test

For a Dixon's test to discriminate the extreme values, the values should be arranged in ascending order. Then, a formula is used in function of the number of the values. For our study, there are four values, the formula used are:

For a minimum

$$x_{min} = \frac{x_2 - x_1}{x_4 - x_1}$$

For a maximum

$$x_{max} = \frac{x_4 - x_3}{x_4 - x_1}$$

If x_{min} or x_{max} is less than $r_{4;0.99}$ (value of the Dixon's table with 4 values and with a threshold of 0.01), the values are not discriminate. If the opposite is true, the extreme value (x_{min} or x_{max}) is removed.

For the ED, the different values which are removed are crossed out on the table S2. For example, the blocking temperature T_B of $S4_{1B}$ is removed compared to the other T_B values of the other samples S4.

Table S3: ANOVA values of the experiments from the ED of the same operator (ED_{1A}, ED_{2A} and ED_{3A}) to check the repeatability of the ED (Repeat = limit of the repeatability, Sd = standard deviation). The difference between each ED is calculated and compare to the limit of the repeatability: if this difference is below to the limit (green value), the experiments are repeatable.

		S1	S2	S3	S4	S5	S6	S7	S8	S9	S10	S11	S12	S13	S14	S15	S16
d_{TEM} (nm)	Repeat	0.14	0.37	0.89	0.56	0.71	0.52	0.60	0.15	0.41	0.33	0.29	0.39	0.53	0.36	0.20	0.44
	Sd	0.05	0.13	0.32	0.20	0.25	0.18	0.21	0.05	0.15	0.12	0.10	0.14	0.19	0.13	0.07	0.16
	1A vs 2A	0.08	0.26	0.21	0.39	0.34	0.25	0.32	0.10	0.29	0.02	0.07	0.25	0.24	0.24	0.08	0.27
	1A vs 3A	0.01	0.15	0.62	0.15	0.15	0.36	0.40	0.02	0.13	0.21	0.20	0.02	0.37	0.04	0.06	0.00
	2A vs 3A	0.09	0.11	0.41	0.24	0.49	0.11	0.08	0.08	0.16	0.19	0.13	0.23	0.13	0.20	0.14	0.27
σ_{TEM} (nm)	Repeat	0.15	0.36	0.29	0.17	0.48	0.07	0.43	0.41	0.45	0.04	0.37	0.48	0.47	0.35	0.38	0.58
	Sd	0.05	0.13	0.10	0.06	0.17	0.03	0.15	0.14	0.16	0.01	0.13	0.17	0.17	0.13	0.13	0.21
	1A vs 2A	0.08	0.25	0.20	0.01	0.01	0.04	0.02	0.26	0.17	-	0.05	0.34	0.26	0.12	0.02	0.28
	1A vs 3A	0.10	0.17	0.13	0.11	0.30	0.05	0.25	0.24	0.15	-	0.20	0.16	0.31	0.25	0.24	0.12
	2A vs 3A	0.02	0.08	0.07	0.10	0.29	0.01	0.27	0.02	0.32	0.02	0.25	0.18	0.05	0.13	0.22	0.40
d_{hydro} (nm)	Repeat	2.02	4.98	2.22	3.31	6.25	3.56	0.55	5.99	10.61	2.91	8.78	3.89	1.63	4.08	2.34	4.04
	Sd	0.71	1.76	0.79	1.17	2.21	1.26	0.20	2.12	3.75	1.03	3.10	1.37	0.58	1.44	0.83	1.43
	1A vs 2A	1.39	3.50	1.57	1.21	3.95	1.99	0.31	2.76	1.79	0.52	2.85	0.59	1.10	2.88	1.22	0.87
	1A vs 3A	0.97	2.06	0.74	1.13	3.68	0.34	0.36	4.16	5.41	1.98	6.20	2.62	0.25	1.29	0.36	2.79
	2A vs 3A	0.42	1.44	0.83	2.34	0.27	2.33	0.05	1.40	7.20	1.46	3.35	2.03	0.85	1.59	1.58	1.92
a_{XRD} (Å)	Repeat	0.07	0.00	0.06	0.06	0.05	0.11	0.08	0.06	0.01	0.03	0.02	0.05	0.03	0.04	0.00	0.06
	Sd	0.02	0.00	0.02	0.02	0.02	0.04	0.03	0.02	0.00	0.01	0.01	0.02	0.01	0.02	0.00	0.02
	1A vs 2A	0.01	0.00	0.02	0.02	0.03	0.04	0.01	0.01	0.00	0.01	0.00	0.02	0.02	0.02	0.00	0.04
	1A vs 3A	0.04	-	0.04	0.04	0.02	0.03	0.04	0.04	0.01	0.01	0.02	0.01	0.01	0.03	-	0.02
	2A vs 3A	0.05	-	0.02	0.03	0.01	0.08	0.05	0.03	0.01	0.02	0.02	0.03	0.01	0.01	-	0.02
t_{XRD} (nm)	Repeat	0.22	0.62	0.35	0.67	0.42	0.70	0.11	0.44	0.58	0.27	1.58	0.22	0.61	0.45	0.41	0.71
	Sd	0.08	0.22	0.13	0.24	0.15	0.25	0.04	0.16	0.21	0.10	0.56	0.08	0.22	0.16	0.15	0.25
	1A vs 2A	0.04	0.27	0.12	0.46	0.15	0.30	0.04	0.23	0.41	0.08	-	0.10	0.41	0.29	0.23	0.23

	1A vs 3A	0.11	0.43	0.13	0.32	0.15	0.19	0.08	0.07	0.24	0.11	0.79	0.15	0.32	0.26	0.27	0.50
	2A vs 3A	0.15	0.16	0.25	0.14	0.30	0.49	0.04	0.30	0.17	0.19	-	0.05	0.09	0.03	0.04	0.27
$\%_{lig}$ (%)	Repeat	0.00	7.49	31.04	17.29	10.20	13.07	15.76	30.26	20.08	2.83	9.94	8.49	8.49	0.00	18.84	11.44
	Sd	0.00	2.65	10.97	6.11	3.61	4.62	5.57	10.69	7.09	1.00	3.51	3.00	3.00	0.00	6.66	4.04
	1A vs 2A	-	1.00	19.00	8.00	2.00	8.00	11.00	18.00	9.00	2.00	7.00	3.00	6.00	0.00	11.00	3.00
	1A vs 3A	-	5.00	0.00	12.00	7.00	8.00	4.00	19.00	5.00	1.00	3.00	3.00	3.00	0.00	1.00	5.00
	2A vs 3A	0.00	4.00	19.00	4.00	5.00	0.00	7.00	1.00	14.00	1.00	4.00	6.00	3.00	0.00	12.00	8.00
M_S 300K ($emu.g^{-1}$)	Repeat	19.05	34.61	11.21	12.44	30.83	3.08	19.15	8.23	14.40	5.32	63.75	15.09	12.33	14.89	11.21	20.03
	Sd	6.73	12.23	3.96	4.40	10.89	1.09	6.77	2.91	5.09	1.88	22.53	5.33	4.36	5.26	3.96	7.08
	1A vs 2A	6.69	18.62	7.57	0.01	17.07	-	13.51	3.50	9.85	3.70	42.36	5.45	8.05	9.95	3.70	13.38
	1A vs 3A	6.77	23.05	1.76	7.61	20.26	1.54	6.11	5.77	2.70	2.44	34.47	10.66	6.91	7.95	4.22	2.68
	2A vs 3A	13.46	4.43	5.81	7.62	3.19	-	7.40	2.27	7.15	1.26	7.89	5.21	1.14	2.00	7.92	10.70
M_S 5K ($emu.g^{-1}$)	Repeat	19.00	28.08	4.86	6.64	26.82	41.91	12.60	3.12	5.13	3.86	49.63	6.31	5.87	17.48	5.40	25.38
	Sd	6.71	9.92	1.72	2.35	9.48	14.81	4.45	1.10	1.81	1.37	17.54	2.23	2.07	6.18	1.91	8.97
	1A vs 2A	12.00	16.06	3.37	1.25	16.68	24.24	8.86	1.92	3.40	2.45	30.73	1.23	3.72	12.29	0.65	15.61

	1A vs 3A	0.78	18.12	1.11	3.29	16.13	2.62	3.65	0.02	0.61	2.27	30.01	4.33	3.45	7.21	3.58	0.15
	2A vs 3A	11.22	2.06	2.26	4.54	0.55	26.86	5.21	1.90	2.79	0.18	0.72	3.10	0.27	5.08	2.93	15.46
T_B (K)	Repeat	9.94	1.63	32.80	6.11	3.27	8.65	16.58	53.12	10.71	7.49	8.65	6.54	4.90	1.63	11.44	4.32
	Sd	3.51	0.58	11.59	2.16	1.15	3.06	5.86	18.77	3.79	2.65	3.06	2.31	1.73	0.58	4.04	1.53
	1A vs 2A	3.00	1.00	19.00	1.00	2.00	6.00	11.00	33.00	6.00	5.00	6.00	0.00	3.00	0.00	7.00	3.00
	1A vs 3A	7.00	0.00	2.00	2.00	0.00	4.00	2.00	32.00	1.00	4.00	2.00	4.00	3.00	1.00	0.00	2.00
	2A vs 3A	4.00	1.00	21.00	3.00	2.00	2.00	9.00	1.00	7.00	1.00	4.00	4.00	0.00	1.00	7.00	1.00

Table S4: ANOVA values of the experiments from the ED from two different operators (ED_{1A} and ED_{1B}) to check the reproducibility of the ED (Repro = limit of the reproducibility, Sd = standard deviation). The difference between the two experiments is calculated and compare with the limit.

		S1	S2	S3	S4	S5	S6	S7	S8	S9	S10	S11	S12	S13	S14	S15	S16
d_{TEM} (nm)	Repro	0.15	0.28	0.52	0.40	0.44	0.66	0.50	0.94	0.47	0.81	0.26	0.57	0.51	0.22	0.57	0.34
	Sd	0.05	0.10	0.19	0.14	0.15	0.23	0.18	0.33	0.16	0.29	0.09	0.20	0.18	0.08	0.20	0.12
	1A vs 1B	0.04	0.23	0.23	0.30	0.14	0.09	0.42	0.43	0.34	0.47	0.01	0.35	0.41	0.06	0.27	0.20
σ_{TEM} (nm)	Repro	0.09	0.28	0.41	0.37	0.31	0.13	0.56	0.27	0.43	0.02	0.47	0.41	0.28	0.31	0.33	0.42
	Sd	0.03	0.10	0.15	0.13	0.11	0.05	0.20	0.10	0.15	0.01	0.17	0.15	0.10	0.11	0.12	0.15
	1A vs 1B	0.06	0.05	0.08	0.22	0.04	0.03	0.33	0.10	0.18	-	0.26	0.32	0.15	0.01	0.21	0.18
d_{hydro} (nm)	Repro	4.60	5.35	2.58	2.01	3.92	2.48	3.14	34.47	7.87	2.67	9.40	3.39	1.03	2.44	3.78	2.55
	Sd	1.63	1.89	0.91	0.71	1.38	0.88	1.11	12.18	2.78	0.94	3.32	1.20	0.36	0.86	1.34	0.90
	1A vs 1B	3.01	0.40	0.35	0.33	1.78	1.24	1.34	14.83	1.26	1.87	6.97	2.34	0.66	1.07	2.05	0.70
a_{XRD} (Å)	Repro	0.04	0.00	0.04	0.05	0.03	0.06	0.05	0.04	0.04	0.03	0.02	0.04	0.02	0.03	0.00	0.03
	Sd	0.01	0.00	0.01	0.02	0.01	0.02	0.02	0.01	0.01	0.01	0.01	0.01	0.01	0.01	0.00	0.01
	1A vs 1B	0.01	0.00	0.01	0.00	0.01	0.00	0.00	0.02	0.02	0.01	0.01	0.01	0.01	0.01	0.00	0.02
t_{XRD} (nm)	Repro	1.04	0.67	0.40	0.43	0.67	0.44	0.23	0.37	0.68	0.25	1.06	0.30	0.58	1.01	0.40	0.59
	Sd	0.37	0.24	0.14	0.15	0.24	0.15	0.08	0.13	0.24	0.09	0.38	0.11	0.21	0.36	0.14	0.21
	1A vs 1B	0.54	0.52	0.17	0.16	0.31	0.12	0.07	0.08	0.51	0.11	0.75	0.22	0.01	0.67	0.33	0.03
%lig (%)	Repro	0.00	14.66	19.37	22.96	9.94	7.58	9.31	22.82	11.89	18.08	22.10	20.60	4.90	4.00	20.47	7.40
	Sd	0.00	5.18	6.84	8.11	3.51	2.68	3.29	8.06	4.20	6.39	7.81	7.28	1.73	1.41	7.23	2.61
	1A vs 1B	-	9.00	10.00	17.00	1.00	5.00	6.00	5.00	0.00	8.00	14.00	10.00	3.00	2.00	12.00	1.00
M_S 300K ($emu.g^{-1}$)	Repro	16.48	31.26	8.01	13.22	24.66	1.87	13.47	18.65	8.36	8.03	48.84	29.82	13.67	12.19	8.16	11.58

	Sd	5.82	11.04	2.83	4.67	8.71	0.66	4.76	6.59	2.95	2.84	17.26	10.54	4.83	4.31	2.88	4.09
	1A vs 1B	6.16	25.90	5.47	8.08	20.97	1.30	10.39	5.92	3.77	1.66	41.65	8.88	10.82	1.65	2.31	5.08
M_S 5K ($emu.g^{-1}$)	Repro	15.36	26.87	3.43	9.47	38.24	28.00	15.43	20.64	4.21	2.23	50.44	32.27	43.30	10.87	24.95	37.12
	Sd	5.43	9.49	1.21	3.35	13.51	9.89	5.45	7.29	1.49	0.79	17.82	11.40	15.30	3.84	8.82	13.12
	1A vs 1B	1.11	22.10	0.51	5.01	28.41	14.25	10.97	10.92	2.83	1.52	40.99	14.17	23.96	4.48	13.78	11.79
T_B (K)	Repro	18.27	60.71	20.08	-	6.93	5.17	10.14	30.70	6.33	16.58	15.50	19.05	6.64	2.83	13.12	3.65
	Sd	6.45	21.45	7.09	-	2.45	1.83	3.58	10.85	2.24	5.86	5.48	6.73	2.35	1.00	4.64	1.29
	1A vs 1B	12.00	30.00	9.00	-	4.00	4.00	6.00	21.00	1.00	5.00	10.00	8.00	5.00	1.00	8.00	3.00

Table S5: average of the different responses of the ED for each level of each factor.

Factor with the level	d_{TEM} (nm)	σ_{TEM} (nm)	d_{hydro} (nm)	a_{XRD} (Å)	t_{XRD} (nm)	$\%_{lig}$ (%)	M_s 300K (emu.g^{-1})	M_s 5K (emu.g^{-1})	T_B (K)
A1	3.05	0.99	8.08	8.386	3.63	28	51.55	72.49	17
A2	3.03	1.02	9.05	8.386	3.56	30	52.22	70.19	18
A3	3.03	1.03	8.22	8.386	3.68	32	52.04	73.41	16
A4	3.01	1.02	8.21	8.380	3.67	33	53.85	74.58	14
B1	2.98	1.07	8.18	8.384	3.63	31	48.01	70.95	15
B2	3.00	0.94	7.69	8.386	3.50	33	50.62	69.83	14
B3	3.09	0.99	8.42	8.386	3.72	29	55.58	74.83	18
B4	3.07	1.04	9.26	8.381	3.70	30	55.46	75.07	17
C1	3.02	1.02	8.30	8.386	3.56	32	48.78	67.13	15
C2	2.98	1.02	7.95	8.387	3.62	31	51.68	71.11	15
C3	3.05	1.04	9.62	8.382	3.68	30	53.42	75.13	18
C4	3.08	0.98	7.68	8.382	3.68	30	55.78	77.31	16
D1	2.99	1.06	7.79	8.384	3.55	30	51.15	72.20	16
D2	3.02	1.02	9.86	8.385	3.79	31	51.73	74.05	17
D3	3.07	0.98	8.05	8.382	3.60	32	52.77	72.86	16
D4	3.05	1.00	7.85	8.386	3.60	30	54.03	71.57	15
E1	2.99	1.00	9.45	8.387	3.65	29	54.82	74.84	19
E2	3.05	1.03	7.77	8.385	3.59	30	53.45	74.15	15
E3	3.08	1.01	8.05	8.385	3.58	31	52.76	72.23	16
E4	3.00	1.01	8.29	8.380	3.71	33	48.64	69.45	14

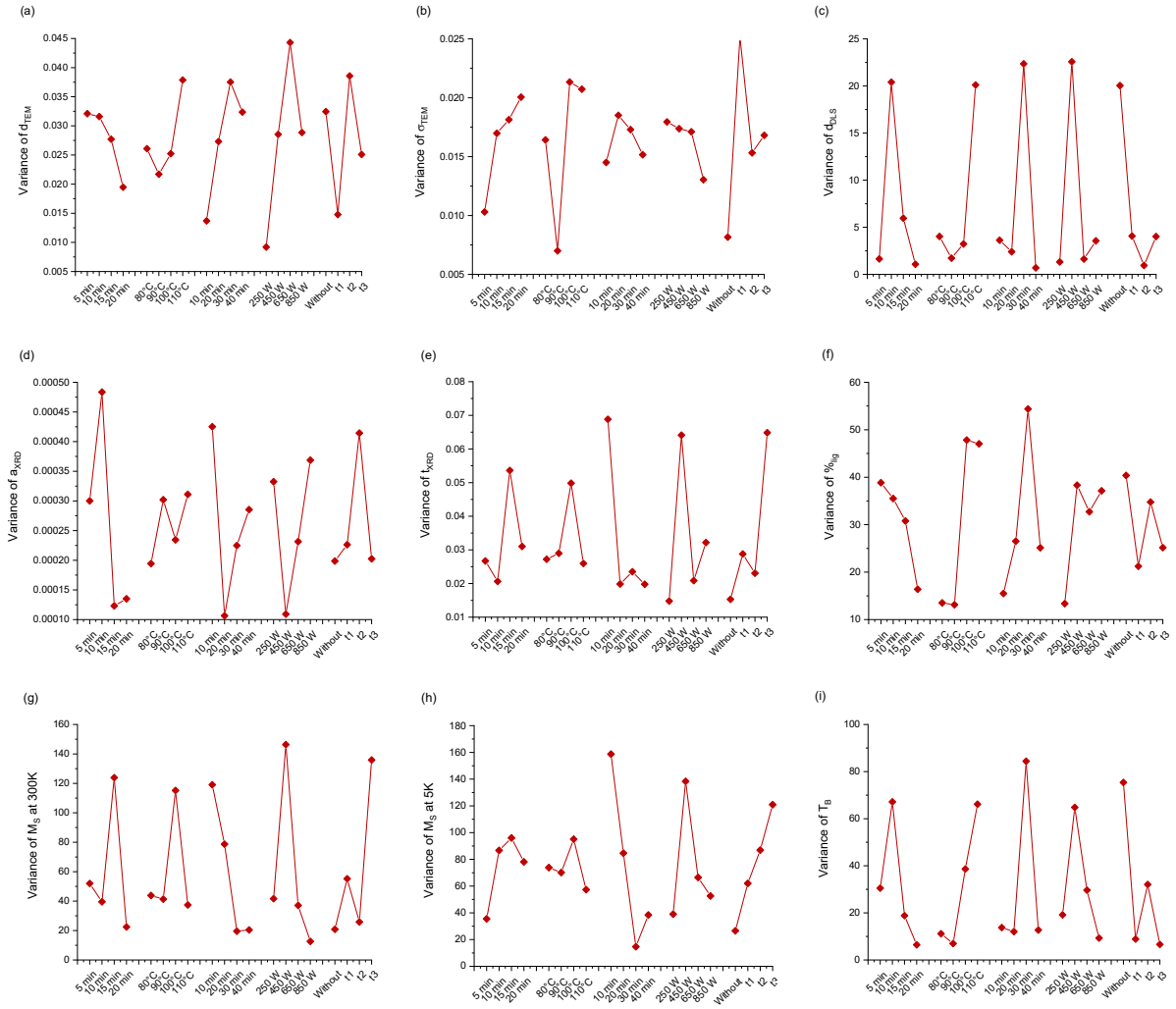

Figure S9: variance diagrams of each responses of the ED in function the level of each factors (the mean diameter d_{TEM} (a), the standard deviation σ_{TEM} (b), the hydrodynamic diameter d_{DLS} (c), the lattice parameter a_{XRD} (d), the crystallite size d_{XRD} (e), the percentage of ligands $\%_{lig}$ (f), the magnetization saturation at 300K M_S_300K (g), at 5K M_S_5K (h) and the blocking temperature T_B (i)).

Table S6: Variation of each factor (time of the ramp, temperature, time of the stage, microwave power, moment of the stirring) in function of the different responses. In these different graphs, all factors are fixed expect one (this one shown on the graph). The values of the graphs are obtained from the simulated data (i.e. from the 1024 simulated experiments).

	Factor A	Factor B	Factor C	Factor D	Factor E
d_{TEM} (nm)	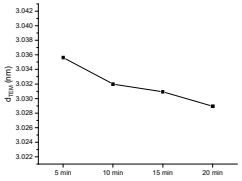	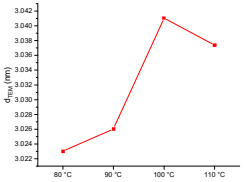	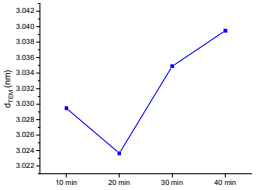	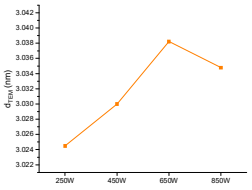	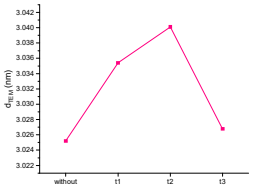
σ_{TEM} (nm)	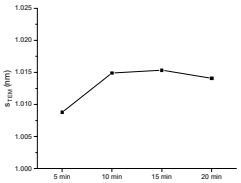	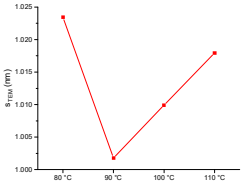	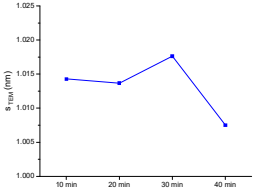	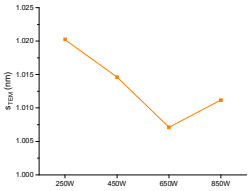	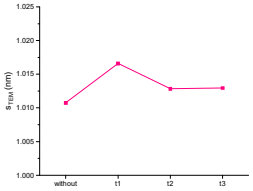
d_{hydro} (nm)	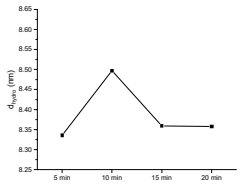	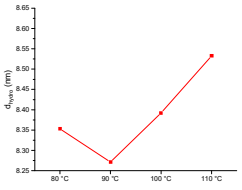	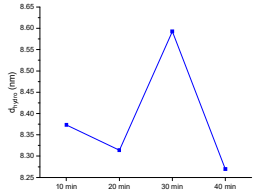	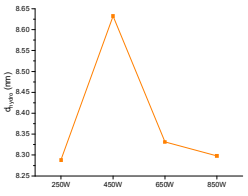	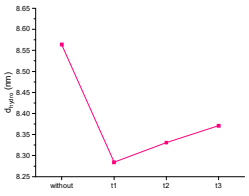
a_{XRD} (Å)	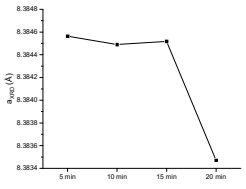	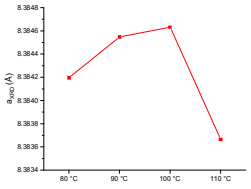	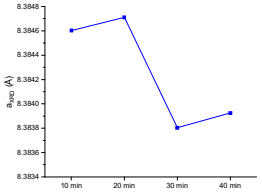	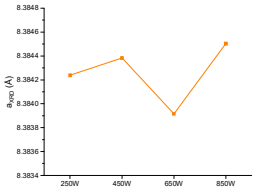	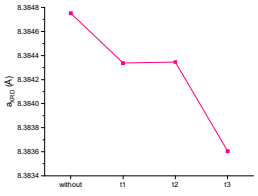

t_{XRD} (nm)	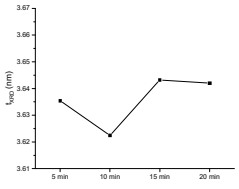	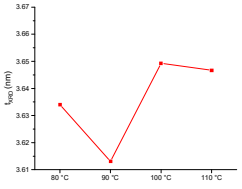	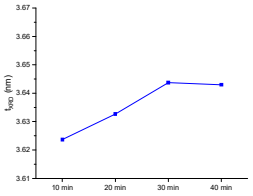	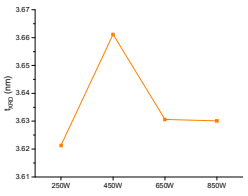	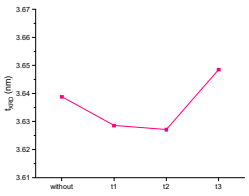
$\%_{lig}$ (%)	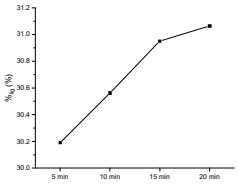	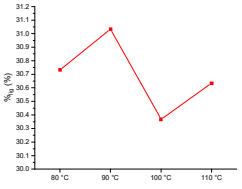	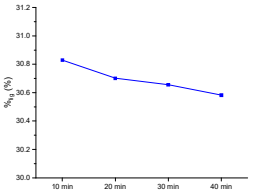	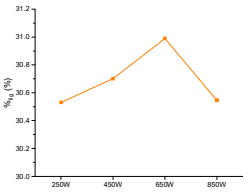	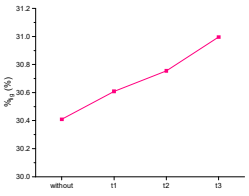
M_s 300K (emu .g^{-1})	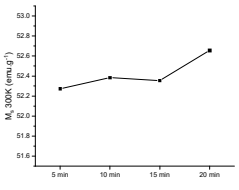	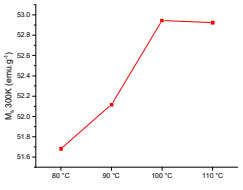	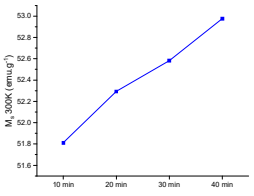	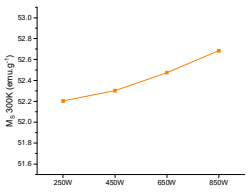	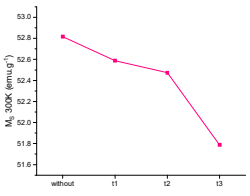
M_s 5K (emu .g^{-1})	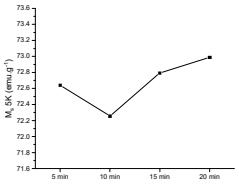	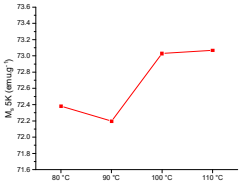	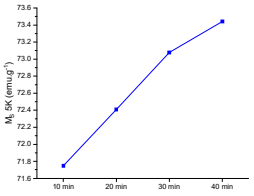	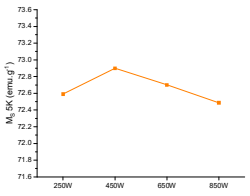	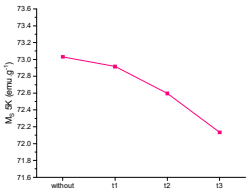
T_B (K)	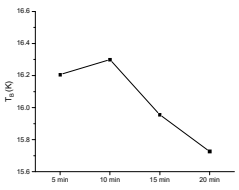	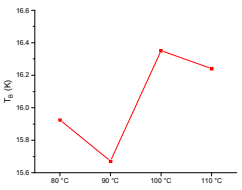	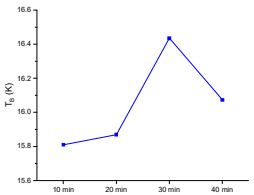	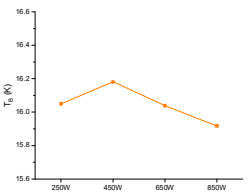	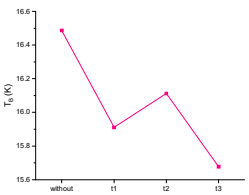

Table S7: table of the microwave parameters of experiments to validate the ED. The first three were chosen at random. The last three were chosen for their optimized responses.

Samples	A	B	C	D	E
S_{50}	1	1	4	1	2
S_{477}	2	4	2	4	1
S_{753}	3	4	4	1	1
S_{893}	4	2	4	4	1
S_{957}	4	3	4	4	1
S_{1021}	4	4	4	4	1

Table S8: summarize of the different responses (theoretical in red and experimental in black) of the experiments to validate the ED.

Sample	d_{TEM} (nm)	σ_{TEM} (nm)	d_{hydro} (nm)	a_{XRD} (Å)	t_{XRD} (nm)	$\%_{lig}$ (%)	M_s 300K (emu.g^{-1})	M_s 5K (emu.g^{-1})	T_B (K)
$S_{50\ theo}$	3.03	1.02	7.98	8.3842	3.62	30	52.06	73.29	16
$S_{50\ exp}$	2.98	1.05	8.57	8.3789	3.17	34	52.11	74.42	14
$S_{477\ theo}$	3.03	1.02	8.66	8.3851	3.63	30	53.44	72.57	17
$S_{477\ exp}$	2.69	0.96	57.28	8.3785	2.48	40	12.08	37.56	11
$S_{753\ theo}$	3.03	1.02	8.46	8.3841	3.65	30	53.61	74.25	17
$S_{753\ exp}$	3.10	0.81	7.90	8.3946	3.66	35	60.83	81.93	15
$S_{893\ theo}$	3.03	0.99	8.21	8.3842	3.62	31	53.58	73.47	16
$S_{893\ exp}$	2.84	0.88	8.46	8.3818	3.40	32	59.30	80.37	13
$S_{957\ theo}$	3.04	1.00	8.33	8.3842	3.66	30	54.41	74.30	16
$S_{957\ exp}$	3.19	0.74	9.03	8.3729	3.49	32	53.83	74.30	14
$S_{1021\ theo}$	3.04	1.01	8.47	8.3833	3.66	30	54.39	74.34	16
$S_{1021\ exp}$	3.15	0.99	5.83	8.3852	3.34	26	38.59	57.67	16